Applied Physics Reviews REVIEW pubs.aip.org/aip/are

Current status and challenges for hole-selective poly-silicon based passivating contacts

Cite as: Appl. Phys. Rev. **11**, 011311 (2024); doi: 10.1063/5.0185379
Submitted: 30 October 2023 · Accepted: 12 January 2024 ·
Published Online: 9 February 2024

Rabin Basnet,[1,a)] Di Yan,[2] Di Kang,[1] Mohamed M. Shehata,[1] Pheng Phang,[1] Thien Truong,[1] James Bullock,[2] Heping Shen,[1] and Daniel Macdonald[1,a)]

AFFILIATIONS

[1]School of Engineering, The Australian National University, Canberra ACT 2601, Australia
[2]Department of Electrical and Electronic Engineering, University of Melbourne, Victoria 3010, Australia

[a)]Authors to whom correspondence should be addressed: rabin.basnet@anu.edu.au and Daniel.macdonald@anu.edu.au

ABSTRACT

Doped polysilicon (poly-Si) passivating contacts have emerged as a key technology for the next generation of silicon solar cells in mass production, owing to their excellent performance and high compatibility with the existing passivated emitter and rear cell technology. However, the current solar cell architecture based on a rear-side electron-selective (n^+) poly-Si contact is also approaching its practical limit (~26%) in mass production. The full potential of doped poly-Si passivating contacts can only be realized through incorporation of both electron-selective and hole-selective (p^+) poly-Si contacts. While studies of both p^+ and n^+ poly-Si contacts commenced simultaneously, significant performance differences have arisen. Phosphorus-doped poly-Si contacts consistently outperform boron-doped counterparts, displaying typically lower recombination current density (J_0) values (1–5 fA/cm^2 vs 7–15 fA/cm^2). This discrepancy can be attributed to inadequate optimization of p^+ poly-Si contacts and fundamental limitations related to boron doping. The poorer passivation of p^+ poly-Si contacts can be at least partly attributed to boron segregation into the interfacial oxide layers, compromising the interfacial oxide integrity and reducing the chemical passivation effectiveness. This review critically examines the progress of p^+ poly-Si contacts characterized by cell efficiency and J_0 values, delves into existing challenges, identifies potential solutions, and explores some potential solar cell architectures to enhance efficiency by incorporating p^+ poly-Si contacts.

TABLE OF CONTENTS

I. INTRODUCTION . . . 1
II. CURRENT STATUS . . . 2
A. Brief overview of formation of p^+ poly-Si contacts . . . 2
B. Gettering by p^+ poly-Si contacts . . . 5
III. CHALLENGES FOR P^+ POLY-SI CONTACTS AND POTENTIAL MITIGATION STRATEGIES . . . 5
A. Boron-induced damage in SiO_x interlayers . . . 5
1. Mitigation strategies of boron-related limitation . . . 5
B. Passivation performance on textured surfaces . . . 9
1. Mitigation strategies . . . 9
C. Amorphization during *in situ* doping . . . 9
D. Screen-printed and fire-through metallization . . . 10
IV. FUTURE OUTLOOK . . . 10
V. CONCLUSION . . . 11

I. INTRODUCTION

Silicon photovoltaics (Si-PV) has become a key technology in the global shift toward clean and sustainable energy. The rapid adoption of Si-PV has been driven by continuous innovations across the entire value chain. Currently, the passivated emitter and rear cell (PERC) technology [Fig. 1(b)] is the workhorse of the Si-PV market because of its ability to achieve higher cost-to-performance ratio than its predecessor, the aluminum back surface field (Al-BSF) cell technology [Fig. 1(a)].[1] Continuous improvements in wafer quality, stability, and production tools have led to consistent improvements in PERC solar cell efficiency in mass production. These developments have now brought PERC solar cell efficiency of 24.5% in the laboratory and average 23.5% in mass production bringing it closer to its practical limit of achievable efficiency, around 24.5% for this architecture.[2–5] To overcome the inherent efficiency limitation mainly due to recombination at the metal contacts of the PERC technology, passivating contact solar cell technologies have emerged as the next generation of solar cells for

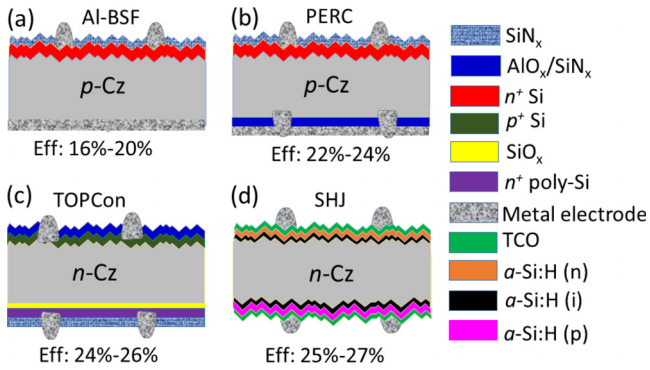

FIG. 1. Schematic of the conventional (a) Al-BSF, (b) PERC, (c) TOPCon, and (d) SHJ solar cell technology. The efficiency ranges are likely ultimate efficiency values for each technology based on current understanding.[11] The thicknesses of individual layers are not up to scale.

mass production. The doped poly-Si films with a thin oxide interlayer the commonly known as tunnel oxide passivated contact (TOPCon) cell technology[6,7] [Fig. 1(c)], have emerged as industrially viable option due to their compatibility with the existing PERC technology.[1] Additionally, doped hydrogenated amorphous (a-Si) silicon heterojunction (SHJ) cell technology[8,9] [Fig. 1(d)], has also remained in the race for next generation of industrial solar cells. However, SHJ cell technology which currently holds the single junction crystalline silicon record at 26.8%[10] is not covered in this review. This review is focused only on the passivating contacts featuring doped poly-Si films which is expected to gain market share from about 10% in 2022 up to 60% within the next 10 years.[1]

Doped poly-Si contacts are formed by inserting an ultrathin silicon oxide (SiO_x) as an interlayer between the crystalline Si wafer and a highly doped poly-Si film. The interfacial oxide layer provides excellent chemical passivation of the dangling bonds and prevents recombination that would otherwise occur at the metal–silicon interface.[12] Additionally, these interlayers enable electrical transport through tunnelling[10–20] and/or pinholes.[24,25] Doped poly-Si films can serve as either electron-selective or hole-selective passivating contacts by doping them n^+ and p^+, respectively. Over the years, extensive research has demonstrated that doped poly-Si contacts can achieve both excellent passivation quality and low contact resistivity (ρ_c) using various interfacial oxide layer and poly-Si deposition methods.[15,26–37] Consequently, many high-efficiency (>25%) silicon solar cells based on doped poly-Si contacts have been demonstrated by research groups and PV manufacturers.[6,38–43] Notably, n^+ poly-Si contacts have consistently shown remarkable performance, with typical single-sided surface recombination current densities (J_0) of less than 5 fA/cm^2 achieved on planar surfaces, regardless of the formation method of the interfacial oxides and the poly-Si layers.[26–29,31,34,44] This underscores the adaptability and robustness of n^+ poly-Si contact fabrication.

The current solar cell architecture based on a rear-side n^+ poly-Si contact (TOPCon) is also approaching its practical limit (~26%) in mass production. A detailed loss analysis of state-of-the-art doped poly-Si solar cells suggested that the recombination loss on the front contacts is one of the main source of efficiency loss.[42,45] Therefore, full potential of poly-Si based passivating contact solar cells could only be realized by incorporating p^+ poly-Si contacts to replace the traditional boron diffused contacts on the front surface. Other report has also concluded that high efficiency solar cells with doped poly-Si passivating contacts will require both n^+ and p^+ poly-Si contacts.[46] That work projected that fully passivating contact solar cells [in this case, the polycrystalline silicon on oxide (POLO) interdigitated back contact architecture] could achieve efficiencies greater than 27.5%, surpassing the limitation of current n-type TOPCon solar cells (26%).[46]

While studies of both p^+ and n^+ poly-Si contacts started around the same time,[47] there has been a notable discrepancy in the progress of their performance. A comparison between the present status of p^+ poly-Si and n^+ poly-Si contacts is shown in Fig. 2(a), based on reported efficiencies of both-sides-contacted solar cells. Numerous research groups and PV manufacturers have consistently demonstrated high-efficiency (>25%) solar cells employing n^+ poly-Si contacts.[6,38–43] The efficiency of solar cells utilizing n^+ poly-Si contacts has shown rapid improvement, with PV manufactures, such as Jinko, Longi, Trina, Jolywood, and DAS solar unveiling impressive efficiency improvements within a short timeframe.[38–41,48] However, progress in the performance of solar cells with p^+ poly-Si contacts has been slower. The record efficiency (23%) of solar cells using only p^+ poly-Si contacts was achieved in 2018.[15] Therefore, there is a significant gap between the performance of p^+ poly-Si contacts and n^+ poly-Si contacts. The primary challenge faced by p^+ poly-Si contacts lies in their comparatively lower surface passivation, typically characterized by J_0 values ranging from 5 to 15 fA/cm^2 on planar surfaces,[21,22,49–52] and their limited compatibility with current screen-printed fire-through metallization processes.

Furthermore, the discrepancy between the performance of n^+ and p^+ poly-Si contacts is also attributed to the inadequate optimization of p^+ poly-Si contacts, as shown in Fig. 2(b). Assuming that each publication related to p^+ poly-Si contacts contribute equally to the understanding and performance advancement, gradual progress hinges on factors such as the number of researchers, their effectiveness, time allocation, and available resources. These factors are often correlated with publication volumes.[53] However, breakthrough single papers may have a more significant impact on the development of the field. Regardless, a comparison of publication counts (peer-reviewed journal articles) related to n^+ poly-Si and p^+ poly-Si contacts since 2014 when the interest in the doped poly-Si contacts was revived, proves instructive. The publication statistics are obtained from publicly available databases, including Scopus, ScienceDirect, and Google Scholar. As illustrated in Fig. 2(b), there are notable disparities on publication volumes between research articles on n^+ poly-Si and p^+ poly-Si contacts, underscoring the more pronounced emphasis and endeavors directed toward the optimization of n^+ poly-Si contacts.

In order to improve the performance of p^+ poly-Si contacts, a comprehensive understanding of their current status and challenges is essential. This review offers an update on the progress of p^+ poly-Si contacts, building upon previous works.[23,72] Subsequently, it will examine the current challenges faced by p^+ poly-Si contacts, explore potential solutions, and provide an outlook of options for the realization of p^+ poly-Si contacts in various high-efficiency solar cell architectures.

II. CURRENT STATUS

A. Brief overview of formation of p^+ poly-Si contacts

The methods commonly employed for the formation of p^+ poly-Si contacts are similar to those used for n^+ poly-Si contacts and have

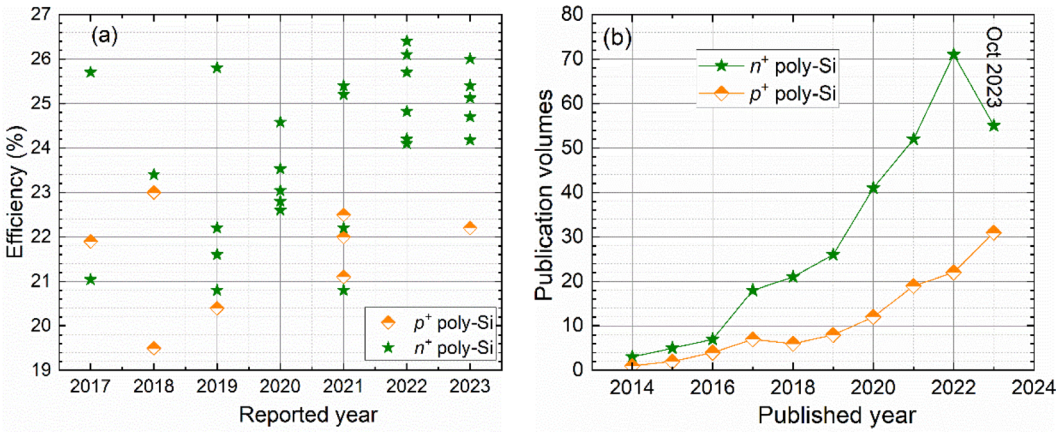

FIG. 2. (a) Reported both-sides-contacted solar cell efficiencies based on p^+ poly-Si contacts and some examples of record cell efficiency based on n^+ poly-Si contacts, including in both laboratories and industry.[15,18–20,23,28,34,39–42,49,54–70] (b) The number of yearly publications related to n^+ poly-Si and p^+ poly-Si contacts were extracted from publically available databases, including Scopus, ScienceDirect, and Google Scholar. Note articles containing both p^+ and n^+ poly-Si contacts are counted for both contacts.

been extensively reviewed elsewhere.[73–76] Here, we will only provide a brief overview of the process flow, as outlined in Fig. 3. Similar to n^+ poly-Si contacts, the formation of p^+ poly-Si contacts also can be divided into five primary steps: (i) growth of the ultrathin interfacial oxide layers, (ii) deposition of intrinsic polycrystalline or amorphous silicon, (iii) crystallization and dopant introduction (*ex situ*) or dopant activation (*in situ*) at an elevated temperature, (iv) hydrogenation, and (v) metallization.

The interfacial oxides can be formed through various methods, including immersion in hot nitric acid,[20,77] UV-assisted ozone oxidation,[36,78] and thermal oxide growth in a furnace at temperatures ranging from 550 °C to 700 °C.[13,17,27,36] *In situ* oxide growth can also be achieved using thermal oxidation followed by chemical vapor deposition (CVD), such as low-pressure CVD (LPCVD) or plasma-enhanced CVD (PECVD).[49,79–81] The type of SiO_x layers has a significant impact on the performance of doped poly-Si contacts, particularly in p^+ poly-Si contacts, as shown in Fig. 4. This is primarily due to boron induced damaged of oxide interlayers due to high levels of B segregation into the SiO_x layers.[82,86] Generally, the typical J_0 values for p^+ poly-Si contacts are in the range of $5-15$ fA/cm^2 on planar wafers, whereas n^+ poly-Si contacts can achieve J_0 values ranging from 1 to 5 fA/cm^2 (Refs. 12, 26, 27, 64, and 84–90) for the same type of oxide layers.

The deposition of intrinsic poly-Si or a-Si layers is primarily carried out using various versions of CVD. LPCVD is the preferred method for n^+ poly-Si in mass production [70% market share in 2023 (Ref. 1)] due to its better uniformity, consistent performance, no blistering, and ease of integration with PERC technology.[13,20,27,36] However, LPCVD is a non-directional double-sided deposition process, which can increase processing costs due to the need to remove the poly-Si layer from one side of the cell, for example, the current TOPCon cells. LPCVD deposited p^+ poly-Si contacts have demonstrated some of the best J_0 values ($1-6.5$ fA/cm^2)[36,44,95,96] as shown in Fig. 4. The one of the lowest J_0 values (1 fA/cm^2) and iV_{oc} of 732 mV for p^+ poly-Si contacts were achieved by thermal oxide as an interlayer with *in situ* boron-doped poly-Si layer deposited by LPCVD and hydrogenated by SiN_x layers.[95] On the other hand, PECVD deposited p^+ poly-Si contacts have also shown promising passivation performance ($J_0 = 3.5$–12 fA/cm^2) comparable to LPCVD.[17,22,49] The single-sided deposition capability of PECVD makes it an attractive option for industry. Nevertheless, PECVD-deposited passivating contacts are susceptible to blistering issues.[71,78,97,98] Beyond PECVD and LPCVD, some studies have explored the use of other methods for forming p^+ poly-Si contacts, such as atmospheric pressure CVD ($J_0 = 6$ fA/cm^2)[99] and hot wire CVD (HWCVD).[100] However, the adoption of these methods is limited to few research laboratories. Another group of methods used for p^+ poly-Si contact formation is physical vapor deposition (PVD), particularly sputtering which has achieved a slightly higher $J_0 = 20$–30 fA/cm^2, which is likely due to sputter damage of

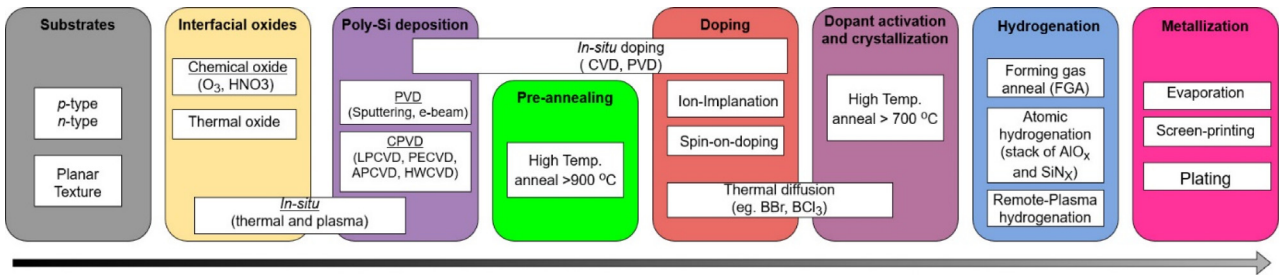

FIG. 3. Schematic of process flows for the formation of p^+ poly-Si contacts.

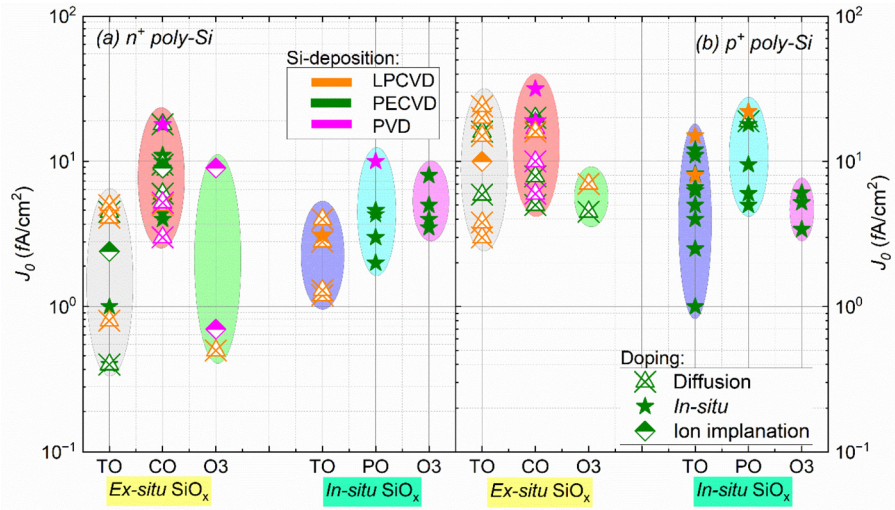

FIG. 4. J_0 values achieved using different techniques to grow the interfacial oxide for (a) n^+ poly-Si contacts and (b) p^+ poly-Si contacts on planar surfaces. Thermal oxide (TO) is dry O_2 thermal oxidation, Chemical oxide (CO) is hot nitric acid oxidation of silicon, Plasma oxide (PO) is O_2 plasma oxidation, and Ozone (O_3) is ozonized water oxidation. *Ex situ* SiO_x, SiO_x is grown in separate processing step; *in situ* SiO_x, SiO_x is grown immediately prior to Si deposition in the same chamber. The shaded shapes provide a guide to the eyes only. These data are adapted from Ref. 75 with updates from Refs. 21, 22, 49, 52, 70, and 91–95.

poly-Si layers.[15,101] However, this single-sided method has increasingly gained attention from the research institutes and PV industries due to the additional benefits of avoiding the use of hazardous precursor gases (such as silane and diborane), eliminating blistering due to a low hydrogen content, and low deposition temperatures.

The doping of poly-Si contacts can be achieved through two broad methods: *ex situ*[13,17,20,102] and *in situ*.[20,22,49] Most research on p^+ poly-Si contacts have focused on *ex situ* doping methods. *Ex situ* doping methods include vapor diffusion (using BCl_3 or BBr_3),[15,101,103,104] ion implantation,[14,105] and liquid-based doping.[14,105–107] Ion implantation and liquid-based doping have also been used to explore alternative doping elements, such as Ga, for the formation of p^+ poly-Si contacts. In *in situ* methods, both the dopant elements and silicon are deposited simultaneously, and the dopant activation is performed in an inert environment at high temperatures. PECVD is considered more suitable for *in situ* deposition of doped poly-Si contacts but is susceptible to hydrogen induced blistering, resulting in a severe degradation of the poly-Si contacts after dopant activation.[47,69,78] Nonetheless, Morisset *et al.*[78] demonstrated that optimizing deposition temperature and gas ratios can yield blister-free p^+ poly-Si contacts by PECVD, achieving one of the best iV_{oc} values of 734 mV for p^+ poly-Si contacts on planar n-type samples ($t = 275\,\mu$m and resistivity $= 2 - 3\,\Omega\cdot$cm).

Following the formation of doped poly-Si contacts, an additional crucial step involves hydrogenation. This step aims to improve the passivation performance of both n^+ and p^+ poly-Si contacts by passivating electronically active dangling bonds at the SiO_x/c-Si interface. Various hydrogenation methods have been explored for doped poly-Si contacts, including the deposition of hydrogen-rich dielectrics such as AlO_x and SiN_x films, as well as annealing in a hydrogen-rich atmosphere (forming gas anneal or remote hydrogen plasma).[21,44,49,50,110,111] Atomic hydrogenation (H-rich dielectric layers or H_2 plasma) has proven to be more effective compared to molecular hydrogenation (FGA).[71,111,112] While hydrogenation is expected to improve the passivation performance of doped poly-Si contacts, recent investigations have demonstrated that excessive hydrogen diffusion could also detrimentally impact their passivation effectiveness.[112,113] Currently, the industrial TOPCon processes do not require an additional hydrogenation step and is achieved during contact firing. The dielectric capping (SiN_x) releases hydrogen into poly-Si contacts. A study by Kang *et al.*[114] revealed that both n^+ and p^+ poly-Si passivating contacts exhibit increased recombination with firing temperature, though the impact on p^+ poly-Si contacts was less severe. The excessive accumulation of hydrogen near the thin interfacial oxide layer was found to significantly degrade the firing stability of n^+ poly-Si contacts, whereas p^+ poly-Si contacts exhibited relatively higher thermal stability over a broader range of hydrogen concentrations. The improved firing stability of p^+ poly-Si contacts can be attributed to their comparatively lower hydrogen diffusivity, leading to slower hydrogen migration[115–118] or to the accumulation of boron at the surface between interfacial SiO_x and Si substrate,[98,123] which could hinder hydrogen diffusion and effusion. However, Mack *et al.*[95] have reported an opposite trend as J_0 values decreased [$J_{0(\text{before firing})} = 13$ fA/cm^2, $J_{0(780\text{C})} = 5$ fA/cm^2, and $J_{0(900\text{C})} = 1$ fA/cm^2] with increased firing temperatures up to 900 °C for *in situ* boron doped p^+ poly-Si contacts with SiN_x as a capping layer.

The formation of metal contacts is achieved through methods such as screen printing,[87,89,90,95,120–126] electroplating,[15] or evaporated metallization.[15,101,104] The Si-PV industry primarily uses screen-printed fire-through metallization.[1] However, contact formation on doped poly-Si contacts presents greater challenges compared to conventional back surface fields. To prevent metal spiking through the oxide interlayer during firing, n^+ poly-Si contacts with a thickness greater than 100 nm have been necessary thus far. This has enabled low contact resistivities $\rho_c \leq 1$ m$\Omega\cdot$cm^2 (Refs. 89, 122, and 125) and low $J_{0,\text{metal}}$ of 30–50 fA/cm^2 (Refs. 87, 89, and 122). However, when applying the same screen-printed and fire-through metallization method to p^+ poly-Si contacts, inferior results have been obtained. Typically, p^+ poly-Si contacts have exhibited higher ρ_c values of 2–10 m$\Omega\cdot$cm^2 and higher $J_{0,\text{metal}}$ values of 160–800 fA/cm^2 (Refs. 95, 120, and 125), even with thicker poly-Si contacts of up to 200 nm. The limited compatibility of p^+ poly-Si contacts with the fire-through metallization process could be partially addressed through further optimization of screen-printed metal paste. Nonetheless, promising outcomes have been observed in the metallization of p^+ poly-Si contacts with evaporated metallization and with low-temperature, non-

fire-through screen-print pastes.[90,124,128] However, these methods are unlikely to be compatible with the mass production metallization of doped poly-Si solar cells.

B. Gettering by p^+ poly-Si contacts

Another benefit of poly-Si contact is its strong impurity gettering effect.[81,103,127–129] The overall gettering effectiveness of the doped poly-Si contact is determined by both the heavily doped poly-Si layers and interfacial oxide layers.[127] Recently, Yang *et al.*[103] provided a comprehensive overview of the gettering effects observed in poly-Si contacts formed using diverse methods, including vapor diffusion, ion-implantation, and *in situ* doping. The study shed light on the distinct mechanisms underlying impurity gettering in both n^+ and p^+ poly-Si contacts. By using iron (Fe) as a tracer impurity, the research demonstrated that the segregation coefficients remained within one order of magnitude for in n^+ poly-Si contacts. However, a much stronger variability in gettering effects was observed in p^+ poly-Si contacts. The study highlighted the strong gettering effects exhibited in vapor-diffused and *in situ* (LPCVD) p^+ poly-Si contacts, surpassing the effects of n^+ poly-Si contacts. In contrast, p^+ poly-Si contacts formed by boron ion-implantation showed relatively weak gettering effects.

III. CHALLENGES FOR p^+ POLY-Si CONTACTS AND POTENTIAL MITIGATION STRATEGIES

As reviewed above, the performance of poly-Si contacts demonstrates a significant dependence on their fabrication processes. However, p^+ poly-Si contacts are consistently inferior to their n^+ counterparts. In the subsequent section, we delve into the fundamental limitations associated with dopant incorporation in p^+ poly-Si contacts, followed by a brief overview of strategies aimed at mitigating these limitations. Additionally, we outline other limitations that primarily stem from inadequate optimization efforts.

A. Boron-induced damage in SiO_x interlayers

The effective operation of passivating contacts relies on the controlled diffusion of dopants from poly-Si layers into the c-Si bulk. Achieving the desired performance of doped poly-Si contacts (J_0 and ρ_c values) hinges on the careful management of peak doping within the poly-Si layers and the subsequent in-diffusion into the c-Si substrate. The observed performance gap between p^+ and n^+ poly-Si contacts can be partially attributed to the distinctive properties of boron (B) and phosphorus (P) in silicon, as shown in Table I. The segregation coefficient of B ($k = 0.1 - 0.3$) is significantly smaller than of P ($k = 10$).[130] As a result, boron accumulates in the oxide interlayer,[82,134,135] which can lead to the degradation of oxide layer and an increase in the density of interface states. Furthermore, the implied solid solubility limit of each dopant in the oxide can be determined from the solid solubility limit in silicon and the segregation coefficient. This is approximately two orders of magnitude higher for B ($0.3 - 1 \times 10^{21}$ cm^{-3}) than for P (2.5×10^{19} cm^{-3}). This implies that the B concentration in the oxide layer is much higher than that of the P concentration. Note the reported segregation coefficients of dopant elements shown in Table I are representative of stoichiometric oxide (SiO_2) layers. However, in realistic conditions, the oxide interlayer might exist in a sub-stoichiometric state, which could further increase the solubility limits. Furthermore, the smaller atomic radius of B (0.087 nm) compared to P (0.098 nm) leads to a greater strain induced by B atoms, leading to the formation of more defects in the oxide interlayer.

1. Mitigation strategies of boron-related limitation

a. Alternative dopant: Ga. To address the damage caused by boron accumulation within the oxide interlayer, Ga has been explored as an alternative doping element.[14,107,119,133] Ga offers advantages such as a much higher segregation coefficient (k) compared to B,[134,135] as shown in Table I. This helps to reduce the accumulation of Ga within the oxide interlayer. Furthermore, the implied solubility of Ga in the oxide is several orders of magnitude lower than that of B, as shown in Table I. Additionally, Ga atoms are significantly larger than B atoms, which minimizes dopant-induced damage to interfacial oxides. Therefore, Ga doping has the potential to improve the passivation performance of p^+ poly-Si contacts.

Young *et al.*[14] conducted a study on the depth profiles of hydrogenated p^+ poly-Si contacts [PECVD *in situ* p^+ (B) poly-Si and ion-implanted p^+ (Ga) poly-Si] through secondary ion mass spectrometry (SIMS), as shown in Fig. 5. The profile illustrates that in p^+ (B) poly-Si contacts, the boron and hydrogen concentrations peaked within the SiO_2 layer, as shown in Fig. 5(a). However, in the case of p^+ (Ga) poly-Si contacts, the Ga distribution does not exhibit a pronounced peak within the SiO_2 layers, as shown in Fig. 5(b). Notably, the p^+ (Ga) poly-Si contacts achieved doping of approximately 2×10^{19} cm^{-3}, consistent with the solid solubility limit of Ga in Si, as shown in Table I. The hydrogen peak is observed only in the p^+ (B) poly-Si contacts, which could be attributed to the hydrogen passivation of oxide/interface defects. Note that the H levels in the c-Si wafer are representative of the background level of the SIMS instrument. In this study, the PECVD *in situ* p^+ (B) poly-Si and ion implanted p^+ (Ga) poly-Si contacts achieved optimal J_0 values of 18 and 1 *f*A/cm^2, respectively, and

TABLE I. Fundamental properties of dopant elements Ga, B, and P in SiO_x and Si at 900 °C.

	Ga	B	P
Segregation coefficient $\{k = \frac{C_{Si}}{C_{SiO_2}}\}$	20 (Ref. 135)	0.1 − 0.3 (Ref. 130)	10 (Ref. 130)
Solid solubility in silicon (cm^{-3})	1.5×10^{19} (Ref.134)	1×10^{20} (Ref. 136)	2.5×10^{20} (Ref.137)
Implied solubility in SiO_2 (cm^{-3})	7.5×10^{17}	$0.3 - 1 \times 10^{21}$	2.5×10^{19}
Atomic radius (nm)	0.136	0.087	0.098
Diffusivity in SiO_2 (cm^2/s)	3×10^{-13} (Ref. 134)	5×10^{-19} (Ref. 134)	9×10^{-12} (Ref. 134)
Diffusivity in Si (cm^2/s)	1×10^{-16} (Ref. 134)	5×10^{-16} (Ref. 134)	3×10^{-16} (Ref. 134)

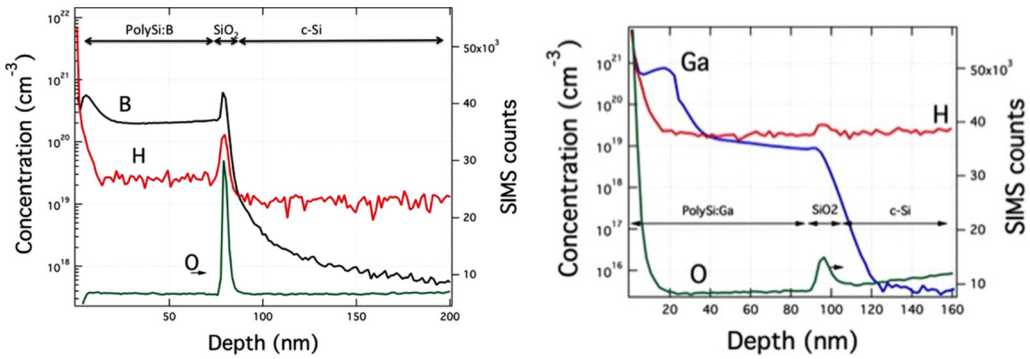

FIG. 5. SIMS depth profile of H, O, (a) B for poly-Si (Ga)/SiO_2 and (b) Ga for poly-Si (B)/SiO_2 passivating contacts. The figures are adapted from Ref. 14 with the permission from National Renewable Energy Laboratory (NREL).

reported an excellent iV_{oc} with a record of 737 mV for p^+ (Ga) poly-Si samples.

However, utilizing Ga also presents inherent challenges for the fabrication of p^+ poly-Si contacts. The diffusivity of Ga in c-Si is slightly smaller than B in c-Si, which can pose difficulties in achieving uniformly doped poly-Si contacts,[134] as shown in Fig. 5(b). Another significant issue arises from the solid solubility of Ga in c-Si, which is nearly one of magnitude lower than of boron at the same diffusion temperature.[134,136] This limitation reduces the achievable dopant concentration in poly-Si contacts, posing a particular challenge in achieving low ρ_c values in doped poly-Si contacts. Thus, the use of non-equilibrium doping methods becomes necessary to activate excess Ga above its solubility limit and achieve a low contact resistivity.[138–140]

Recently, Chen *et al.* employed a nanosecond-scale pulsed laser melting technique to overcome this limitation of conventional thermal processing, enabling doping above the equilibrium solid solubility of Ga in poly-Si layers to form p^+ poly-Si contacts. The study achieved Ga and B concentrations of 3×10^{20} and 1×10^{21} cm^{-3}, respectively, significantly surpassing the solid solubility in c-Si, as shown in Table I. Impressively, the approach led to p^+ (Ga) poly-Si contacts with a low ρ_c value of 35.5 $m\Omega\cdot cm^2$, in contrast to the 2000 $m\Omega\cdot cm^2$ obtained through conventional furnace annealing. Remarkably, the hyper-doped p^+ poly-Si (Ga) contacts maintained a low J_0 value of 4.1 fA/cm^2 ($iV_{oc} = 735$ mV) indicating the absence of laser-induced damage and establishing this method as promising for p^+ poly-Si contacts. It is worth noting that the study utilized relatively a thick poly-Si layer (~ 250 nm), further exploration would be necessary to determine whether the process can maintain performance with thinner poly-Si layers.

Nevertheless, using both B and Ga as dopants presents an opportunity to improve p^+ poly-Si contacts performance, particularly on the rear side of solar cells. One strategy could involve employing p^+ poly-Si (B) contacts in the metal-contacted areas, while employing p^+ (Ga) poly-Si contacts to passivate the non-contacted areas. This dual-doping strategy could help overcome the limitation of each dopant and optimizes the performance of p^+ poly-Si contacts. Truong *et al.*[107] demonstrated co-doping of Ga with B using a spin-on doping method to form p^+ poly-Si passivating contacts. However, they found even a small fraction of B co-doping caused a large reduction in surface passivation. Therefore, an optimization of B and Ga concentration is crucial.

b. Pinhole oxides. Two different models have been established to describe the transport of charge carriers through the oxide interlayers in poly-Si contacts: direct tunneling across the oxide interlayer and drift-diffusion through pinholes in the oxide. It is well-understood that charge carrier predominantly tunnel through ultrathin oxide layers when they are less than 2 nm thick.[141] On the other hand, charge carrier transport through thicker oxide layers (>2 nm) occurs primarily through pinholes formed after a high-temperature annealing ($T > 1000\,°C$).[142] The formation of pinholes upon thermal annealing has been confirmed by several works using various methods such as transmission electron microscopy[142–144] and electron-beam-induced current (EBIC).[144] It is crucial to control pinhole density and size to maintain the high passivation of passivating contacts based on pinhole oxides, commonly referred to as polysilicon on POLO structures.[24,147] In principle, thicker pinhole oxides are expected to be more resilient to boron-induced defects, achieving lower J_0 for p^+ (B) poly-Si contacts. However, published data do not seem to support this expectation, as shown in Fig. 6. The typical J_0 values for pinhole oxides 3–8 fA/cm^2 (Refs. 44 and 90) is within the range of best J_0 values for p^+ (B) poly-Si contacts based on tunneling oxides. It is worth noting that there is limited optimization work conducted on pinhole-based p^+ poly-Si contacts compared to their tunneling-based counterparts, which should be explored further to improve performance.

c. Alternative interfacial layers. The use of SiO_x films as tunneling layers in hole-selective contacts brings inherent drawbacks. The valence band offset of SiO_x layer, which is approximately 4.5 eV, along with the large tunneling effective mass of holes (0.58 m_h) within SiO_x collectively contribute to limited hole tunneling. Consequently, this may result in suboptimal hole-selective contacts compared to electron-selective contacts with conduction band offset of 3.2 eV and smaller tunneling effective mass of electron (0.42 m_e), as shown in Table II. Note that m_e and m_h are the free electron mass and free hole mass, respectively. In response to these challenges, alternative ultrathin tunnel interlayers such as AlO_x and SiN_x films have been explored. These interlayers are interesting due to their exceptional uniformity and thickness control when deposited by atomic layer deposition (ALD).[102,149,150] Furthermore, these interlayers exhibit more favorable valence band offsets with silicon compared to SiO_x, as shown in Fig. 7. It is worth noting the uncertainty regarding the persistence and homogeneity of fixed charges in the ultrathin tunneling dielectric layers after

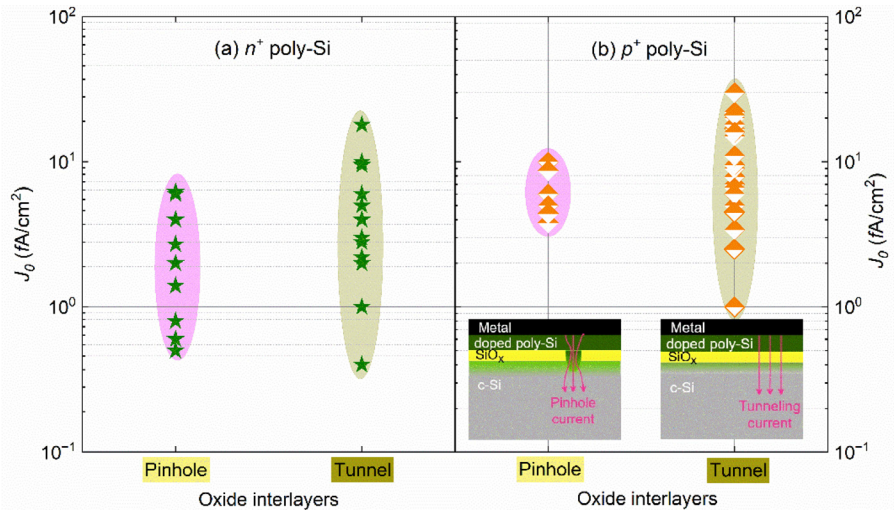

FIG. 6. J_0 values achieved for poly-Si contacts where transport is facilitated predominately by tunneling and pinholes for (a) n^+ poly-Si contacts and (b) p^+ poly-Si contacts on planar surfaces. The inset figures show the schematic of poly-Si contacts based on tunneling and pinhole oxides. These data were extracted from Refs. 21, 22, 24, 36, 44, 70, 75, 87–90, 94, 95, 124, and 146–148.

TABLE II. Literature values of selected properties of SiO_x, SiN_x, and AlO_x layers with thickness below 2 nm when used as an interface with c–Si.

Interlayers	Conduction band offset (eV)	Valence band offset (eV)	Tunneling effective masses	Typical intrinsic charge density (cm^{-2})
SiO_x	3.2 (Ref. 152)	4.5 (Ref. 152)	0.42 m_e, 0.58 m_h (Refs. 153 and 154)	$+9 \times 10^{10}$ (Ref. 150)
SiN_x	2.2 (Ref. 155)	1.8 (Ref. 155)	0.5 m_e, 0.5 m_h	$+1.5 \times 10^{12}$ (Ref. 150)
AlO_x	2.7 (Ref. 156)	3.3 (Ref. 156)	0.4 m_e,0.4 m_h	-4×10^{12} (Ref. 150)

the heavy doping and high temperature processes. Consequently, the influence of the fixed charges is not taken into account when illustrating the band energy diagrams.[151]

However, both SiN_x and AlO_x interlayers can have a high concentration of intrinsic charge, which can impact their performance as hole-selective contacts, as shown in Table II. In the case of AlO_x, the presence of negative charge can create a beneficial accumulation regime in a hole-selective contact. This can improve hole accumulation/transport and facilitate efficient carrier extraction, which is desirable for achieving low ρ_c values. On the other hand, the positive charge in SiN_x interlayers may lead to the generation of a depletion region at the interface. This depletion region can adversely affect the contact properties for hole-selective layers, as it can hinder hole transport and increase ρ_c values. Recent studies have shown promising indications of improvement when incorporating SiN_x and AlO_x interlayers into p^+ poly-Si contacts,[102,149,150,157–159] as shown in Fig. 8. However, further research is needed to explore the advantages and drawbacks of alternative interlayers such as SiN_x and AlO_x, particularly when

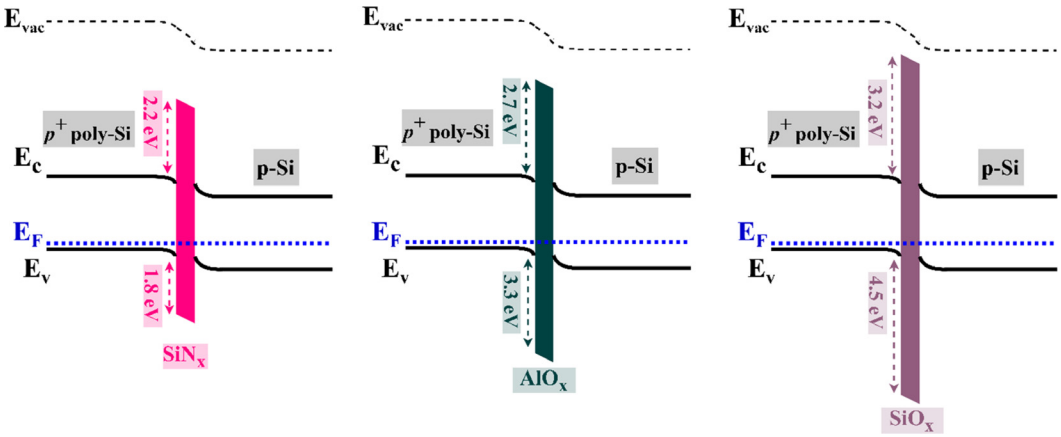

FIG. 7. Potential energy band profiles at equilibrium for p-Si and heavily doped p^+ poly-Si, incorporating various dielectric tunneling interlayers, such as SiN_x, AlO_x, and SiO_x, while also displaying the offsets of these interlayers.

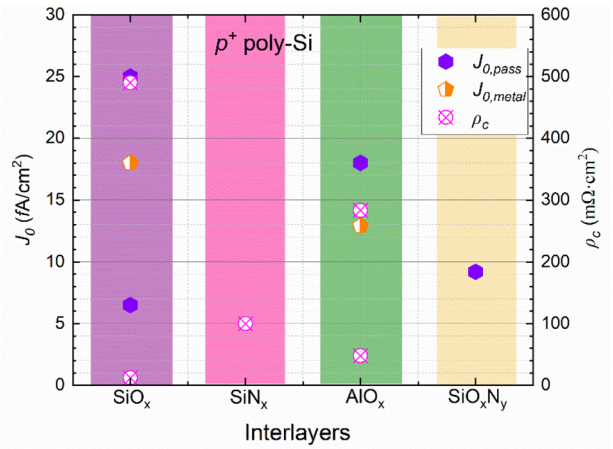

FIG. 8. Comparison of J_0, ρ_c, and $J_{0,metal}$ values achieved when the samples were passivated by p^+ poly-Si contacts using different interfacial layers. The data points were obtained from Refs. 107, 156, 162, and 165–167.

employing ultrathin layers with expectedly lower intrinsic charge compared to bulk films.

Moreover, some of studies have explored the possibility of incorporating nitrogen into SiO_x interlayers, either during N_2O plasma oxidation or through post-nitridation to form silicon oxynitride (SiO_xN_y) layers[74,82] to improve the performance of p^+ poly-Si contacts. These investigations observed less in-diffused boron concentration with SiO_xN_y interlayers. The reduction of boron in-diffused concentration was expected due to a low B segregation coefficient in SiO_xN_y (~20) compared with pure SiO_2 (stoichiometric) interlayers.[160] Some of the studies also suggest that the reduction of in-diffusion is attributed to the formation of B^+-N bonds within the interlayers.[160–162]

d. Multilayer configurations. In recent years, there has been a growing emphasis on controlling the in-diffusion of dopants as a means to improve the performance of doped poly-Si contacts.[96,164,170] One avenue explored involves employing a multilayer system that incorporates additional oxide layers [Fig. 9(b)],[96,109,171] or intrinsic a-Si or poly-Si layers [Fig. 9(c)],[109,140] within the structure of doped poly-Si contacts. The purpose of these approaches is to mitigate the detrimental effects of boron segregation-induced damage on the interfacial oxides.

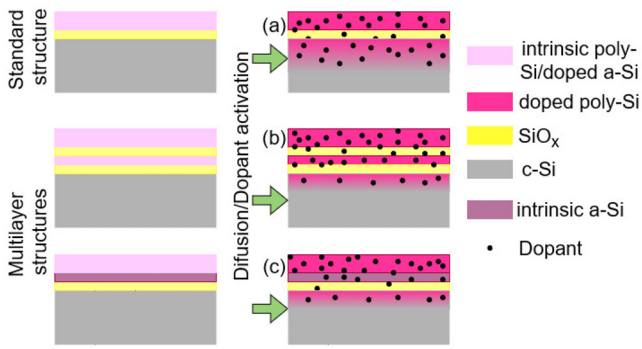

FIG. 9. Schematic of (a) standard doped poly-Si contact and potential multilayer structures consisting of additional (b) oxide layer, and (c) intrinsic a-Si or poly-Si layer to control dopant in-diffusion. The layers' thicknesses are not to the scale.

Stodolny *et al.*[96] conducted a study comparing the performance of p^+ poly-Si contacts using a conventional poly-Si/SiO_x/c-Si [Fig. 9(a)] configuration with a multilayer system that introduced an extra oxide layer positioned at 20 nm from the interface (poly-Si/SiO_x/poly-Si/SiO_x/c-Si) [Fig. 9(b)]. With the introduction of this additional oxide layer, they observed a decrease in the concentration of in-diffused boron from 1×10^{20} cm^{-3} to 6×10^{19} cm^{-3} near the interface, and a reduction in the in-diffused tail depth from 80 to 40 nm. These modifications yielded improvements in J_0 values from 21 to 9 fA/cm^2 on textured surfaces and from 5 to 3 fA/cm^2 on planar surfaces (after hydrogenation). This improvement was primarily attributed to the reduced boron segregation into the interfacial oxide and reduced Auger recombination below the interfacial oxide. Similarly, Polzin *et al.*[109] demonstrated that the insertion of 10–15 nm intrinsic a-Si layers [Fig. 9(c)] resulted in a more uniform boron distribution within p^+ poly-Si contacts, and reduced boron in-diffusion. As a result, the passivation performance was significantly improved from $J_0 = 23$ fA/cm^2 to $J_0 = 11$ fA/cm^2 on planar surfaces.

However, it is important to acknowledge the implementation of a multilayer strategy for forming doped poly-Si contacts, which may be difficult in the industry due to the added complexity and the processing steps. Their impact on the contact resistivity would also need to be carefully monitored.

e. Pre-annealing. The performance of *ex situ* p^+ poly-Si (B) contacts has also seen improvement incorporating a high-temperature pre-annealing step (≥1000 °C) prior to thermal boron diffusion, as shown in Fig. 3. This pre-annealing step serves a dual purpose in enhancing the passivation of doped poly-Si. First, it is believed to impact passivation by promoting stoichiometry of the interfacial oxides.[104] It is widely recognized that the passivation quality of doped poly-Si contacts strongly depends on the stoichiometry of the interfacial oxides.[15,20,104,136,137] Sub-stoichiometric SiO_x layers are more susceptible to disruptions, during high-temperature dopant diffusion processes, particularly during the diffusion of boron.[30,165] Stucklberger *et al.*[104] conducted a comprehensive study investigating the impact of different pre-annealing temperatures (ranging from 850 to 1050 °C) on the performance of LPCVD deposited p^+ poly-Si contacts. Their study demonstrated that a pre-annealing step at 1050 °C during the formation of p^+ poly-Si contacts led to improvements in iV_{oc} of 5–10 and 24 mV on planar and textured (both hydrogenated) samples, respectively.

Second, it is also believed that pre-annealing improves the passivation of doped poly-Si contacts by intentionally generating pinholes in the oxide layer. Yang *et al.*[166] showed that ion-implanted p^+ poly-Si passivated samples with pinholes (pre-annealed) showed a gain of 10 mV in iV_{oc} compared to p^+ poly-Si passivated samples prepared without intentionally pre-forming pinholes (without pre-annealing) on textured samples. However, there is also an optimal pinhole density that could have a minimal impact on the in-diffused doping concentration but a positive effect on the passivation quality.[82,167] A higher pinhole density could increase in-diffusion of dopants and Auger recombination, leading to lower surface passivation. Nevertheless, the sensitivity of the passivation quality to pinhole density for p^+ poly-Si

contacts is much lower than in the case of n^+ poly-Si contacts.[166] This is attributed to the reduction of oxide damage by boron atoms with alternative transport path provided by pinholes.

Furthermore, a good performing doped poly-Si layers could possibly require a crystal size as large as possible. It is known that the during the *ex situ* doping process poly-Si is expected to undergo significant crystal size growth enhancement when doped with phosphorus.[168,169] Consequently, pre-annealing is not crucial for n^+ poly-Si layers to pre-crystallize and increase crystal size. However, crystal size growth enhancement effect is negligible during B doping, particularly when concentration is within the range of $1 \times 10^{19} - 1 \times 10^{21}$ cm^{-3} (Refs. 169–171). Therefore, pre-annealing is also believed to be beneficial for p^+ poly-Si contacts due to enlargement of crystal size prior to B doping.

B. Passivation performance on textured surfaces

The current state-of-the-art TOPCon cells are only textured on the front side. Texturing on the rear-side is desirable for bifacility and improved light trapping as well as wafers become thinner. However, the passivation performance of doped poly-Si contacts is clearly influenced by the surface morphology, as shown in Fig. 10.

The quality of interfacial oxide layers emerges as a pivotal factor in achieving excellent chemical passivation through doped poly-Si contacts. Textured surfaces introduce complexities as the ultrathin SiO_x layers experience disruptions along the peaks and edges of the pyramid features. Additionally, non-uniformity in SiO_x thickness arises from different oxide growth rates on different crystallographic planes, such as <100> and <111>,[172] and this non-uniformity is further accentuated across the peaks and valleys of the textured surface.[173,174] It is worth highlighting that a SiO_x/c-Si interface on <111> exhibits a higher density of interface defect states compared to the SiO_x/c-Si interface on <100>, with values approximately at 10^{10} cm^{-2} eV^{-1} for <100> and 3×10^{11} cm^{-2} eV^{-1} for <111> surfaces.[175,176] Additionally, the sharp edges of the pyramid structures exhibit elevated stress concentration levels,[177] which are known to increase recombination activity.[178,179] These characteristics inherent to textured surfaces collectively contribute to the reduction in their passivation performance with doped poly-Si contacts. These challenges become even more pronounced with the diffusion of boron during the formation of p^+ poly-Si contacts, as shown in Fig. 10.

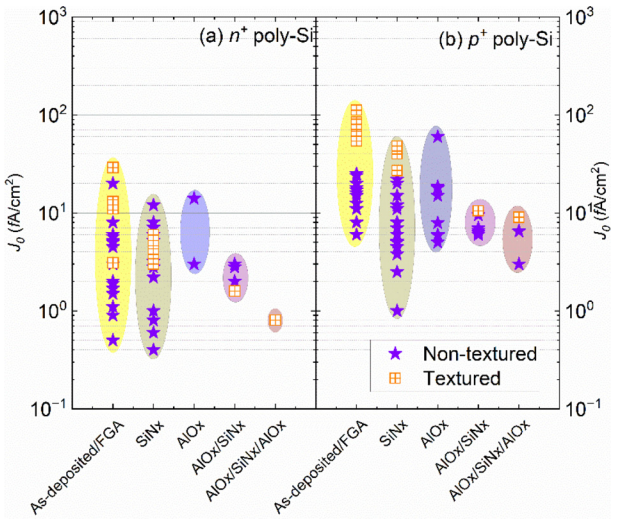

FIG. 10. Comparison of J_0 on planar and textured surfaces passivated by (a) n^+ poly-Si and (b) p^+ poly-Si layers for different hydrogenation schemes as noted in the legend. The shaded shapes provide a guide to the eyes only. These data are adapted from Ref. 75 with new updates from Refs. 21, 49, 49, 50, 70, 91, 94, 95, 106, 108, and 109.

Larionova *et al.*[36] investigated the recombination behavior of p^+ poly-Si contacts on silicon with different crystal orientations, elucidating the poor performance on the textured surfaces. The study reported J_0 values to be 90, 70, and 10 *f*A/cm^2 on <111> planar, <100> textured, and <100> planar surfaces, respectively.

1. Mitigation strategies

Several researchers are actively exploring strategies to address the challenges of doped poly-Si contact passivation performance on both planar and textured surfaces. These strategies encompass optimization of deposition parameters, surface treatments, passivation layer design, and interface engineering technique.[44,96,162–164,180–182] Hydrogenation stands out as a prevalent approach to improve the performance of doped poly-Si contacts on both types of surfaces. Stodolny *et al.*[96] demonstrated advanced hydrogenation schemes, involving novel dielectric stacked layers to improve the passivation of p^+ poly-Si contacts on textured surfaces, yielding J_0 of 44, 21, 15, and 11 *f*A/cm^2 values on textured surfaces before hydrogenation and after hydrogenation with SiN_x, AlO_x/SiN_x, and $AlO_x/SiN_x/AlO_x$ layers, respectively.

Furthermore, Mack *et al.*[180] demonstrated that the utilization of slightly thicker SiO_x layers (while still maintaining tunneling transport characteristics) compared to planar surfaces could yield improved J_0 values on textured surfaces for p^+ poly-Si contacts. Lozac'h *et al.*[181,184] proposed the application of atomic layer deposition (ALD) to create ultrathin SiO_x layers instead of the conventional thermal or chemical SiO_x, affording enhanced control over SiO_x thicknesses across different crystal orientations and ensuring excellent conformal coverage on textured surfaces.

Moreover, other studies have shown that rounding of sharp edges, peaks, and valleys on standard pyramid structures can improve passivation quality without significant loss in optical benefits.[51,65,185,192] Several works have demonstrated that alkaline or acidic polishing selectively polishes the vertices of random pyramid textured surfaces by forming a pyramidical base, resulting to a decreased proportion of Si <111> crystal orientation surfaces.[65,193,194]

C. Amorphization during *in situ* doping

At present, the predominant technique employed in the Si-PV industry to create doped poly-Si contacts uses the LPCVD method coupled with *ex situ* doping. However, the international technology roadmap for PV (ITRPV) predicts a growing preference (50% market share from 2025 onwards) for *in situ* doped poly-Si contacts in the upcoming years, due to not requiring a single-side etch to remove the poly-Si layers from the other side.[1] However, one challenge related to this approach is the amorphization or reduced crystallinity of the poly-Si layers, which can occur during *in situ* B doping.[186] The introduction of B atoms can induce strain and disrupt the crystal structure, ultimately leading to amorphization. This does not occur for n^+ poly-Si

contacts as the larger size of P atoms does not introduce sufficient strain to disrupt the crystal structure.

Typically, reducing the concentration of boron doping helps to mitigate amorphization and enhance carrier mobility in the poly-Si layer during *in situ* B doping. Nevertheless, achieving rapid deposition, uniform coverage over a large area, and the desired dopant concentration of *in situ* B-doped poly-Si contacts simultaneously is a challenge.

D. Screen-printed and fire-through metallization

To date, the metallization of p^+ poly-Si contacts using the conventional screen-printed and fire-through metallization method has not been extensively studied. The majority of research has focused on n^+ poly-Si contacts using Ag pastes, which have been meticulously optimized for mass production. However, screen-printed metallization of p^+ poly-Si contacts still significantly lag n+ poly-Si contacts after metallization, especially in terms of ρ_c values, as shown in Fig. 11.

Typically, the formation of metal contacts with p^+ Si (boron-diffused surfaces) using traditional Ag pastes has yielded a relatively high ρ_c values (>50 mΩ·cm).[187] Studies have shown that the incorporation of Al into the Ag pastes can reduce ρ_c values.[188,189] Nevertheless, the utilization of Ag–Al pastes leads to the growth of substantial metal spikes that penetrate the Si surface to a depth of up to 1 μm. In the co-firing process, the metal pastes must locally permeate the SiN_x capping layers, facilitated by glass frits, to establish a low-Ohmic contact. However, the penetration through the interfacial oxide layers and beyond into the c-Si bulk by the aggressive glass frit and metal spikes must be avoided in order to preserve the outstanding passivation of the doped poly-Si/SiO_x contacts. Recent advances have demonstrated the viability of p^+ poly-Si contact properties through the application of fire-through Ag pastes[95] and Ag–Al pastes.[120,125,190]

Importantly, for similar doped poly-Si thicknesses a wide range of ρ_c and $J_{0,\mathrm{metal}}$ values are achieved across different studies, as shown in Fig. 11. One of the potential reasons for this discrepancy could be attributed to the usage of different metal pastes (different suppliers and chemistry), which appears to heavily influence the performance of doped-poly-Si contacts.

A comprehensive study conducted by Padhamnath *et al.*[121] extensively examined the impact of surface morphology (planar vs textured surface) and poly-Si thickness on the contact formation of p^+ poly-Si, using fire-though Ag-Al pastes. They showed that ρ_c values were poorer on planar surfaces compared to textured surfaces. Furthermore, this difference could not be solely attributed to the increased surface area of textured surfaces. However, the presence of pyramid features was discovered to create disruptions within the glass layer (fired contacts). These disruptions played a crucial role in facilitating the formation of metal crystallites, which are vital for establishing effective contacts. Additionally, the study demonstrated that the ρ_c values increased to 10.5 from 3 mΩ cm^2 when the p^+ poly-Si layer thickness increased from 22 to 235 nm. This phenomenon was primarily ascribed to the penetration of oxide interlayers by the metal crystallites. These observations indicate that the challenge in achieving low ρ_c values of screen-printed metal pastes with p^+ poly-Si contacts lie in the inability to form small, dense, and shallow metal crystallites.

While several paste suppliers have already undertaken the optimization of Ag pastes for n^+ poly-Si contacts, further dedicated effort is required to tailor pastes that are specifically suitable for p^+ poly-Si contacts. These pastes should be designed to restrict the formation of metal crystallites within a few tens of nm in the p^+ poly-Si contacts.

Furthermore, in the context of the Si-PV industry's trajectory toward the multi-terawatt scale, the utilization of Ag screen-printed contacts on both sides of solar cells will depend on the available supply of silver.[192,193] In this context, the electroplating of Ni/Cu/Ag contacts provides a viable pathway to address the challenges associated with screen-printed and fire-through metallization of doped poly-Si solar cells.[194] ITRPV projected that the Cu plating technology could reduce the silver consumption of TOPCon electrodes from 20 mg/W of the screen-printed method to 0.6 mg/W.

IV. FUTURE OUTLOOK

It is understood that the most straightforward pathways to improve the current cell technology is to reduce recombination losses due to metal contacts. High-quality p^+ poly-Si passivating contacts allows this reduction by replacing direct metal-silicon contacts under

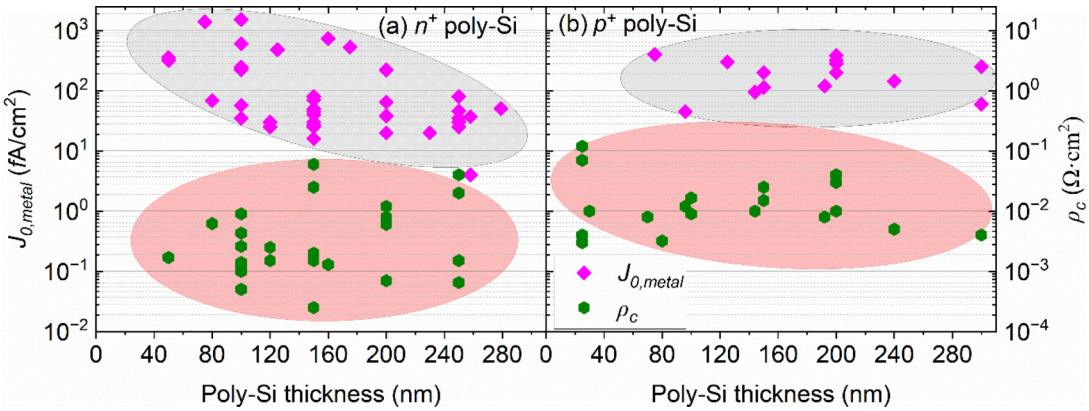

FIG. 11. Recombination on metalized poly-Si contacts ($J_{0,\mathrm{metal}}$) and ρ_c for (a) n^+ poly-Si and (b) p^+ poly-Si contacts as a function of the thickness of the poly-Si layer. The data are for screen-printed metallization either using Ag or Ag–Al pastes. The shaded shapes provide a guide to the eyes only. These data are adapted from Ref. 75 with new updates from Refs. 21–23,51, 52, 70, 91, 121, 183, and 191.

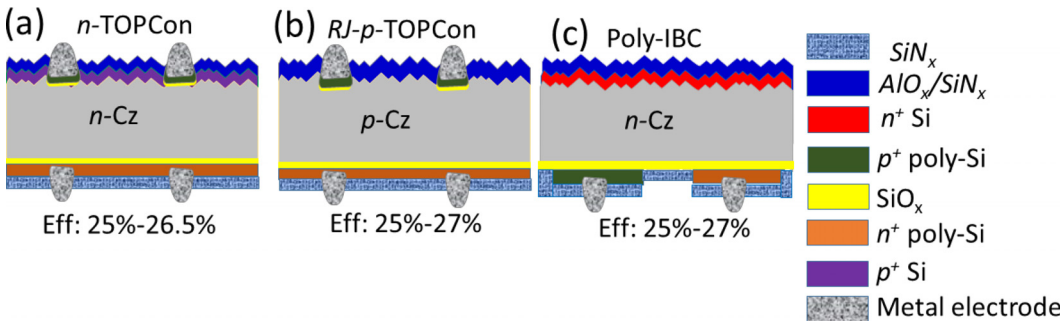

FIG. 12. Schematic of some examples of solar cell structures that can use p^+ poly-Si contacts for the improvement of solar cell performance. (a) Conventional *n*-TOPCon with p^+ poly-Si contacts underneath front metal fingers, (b) rear-junction *p*-TOPCon with p^+ poly-Si contacts underneath front metal fingers, and (c) Poly-IBC structure with p^+ poly-Si contacts on the rear side of the cell. The efficiency range are likely ultimate efficiency values for each technology based on current understanding.[11] The thicknesses of individual layers are not up to scale.

the fingers. It enables many solar cell architectures with high-efficiency potential, some of which are illustrated in Fig. 12. Direct integration of p^+ poly-Si contacts into the current TOPCon structure involves replacing the heavily doped boron-diffused p^{++} Si beneath the front fingers with p^+ poly-Si contacts [Fig. 12(a)] which will help to improve the V_{oc}. This configuration is believed to increase efficiency potential of the TOPCon cell to 26.5%. Moreover, p^+ poly-Si contacts can also be incorporated under the front fingers in *p*-type wafers for the rear-junction (RJ) TOPCon solar cells [Fig. 12(b)]. This technology will be highly sensitive on the quality of *p*-type wafers and has efficiency potential to achieve 27% due to added advantage of fill factor improvement. Interdigitated back contact (IBC) solar cells have demonstrated great potential by incorporating both doped poly-Si contacts on the rear side of the cells[90] [Fig. 12(c)]. The biggest challenges for this cell structure compared to a both-sided-contacted cell structure is the added complexity, with doping and contacts of both polarities on rear-side. Additionally, the utilization of p^+ poly-Si contacts as a top junction of bottom Si cells has been demonstrated in novel high-efficiency perovskite/Si tandem solar cells.[195–197] This structure enables direct contact of electron transport layers, such as titanium oxide (TiO_x) in *n-i-p* perovskite top cells, eliminating the need for additional recombination layers. Optoelectronic modeling of this design has shown tandem cells efficiency potential exceeding 32%.[196] Clearly, the incorporation of high-quality p^+ poly-Si contacts offers numerous potential advantages for upgrading current Si-PV technologies. However, in most cases, achieving this improvement requires the localization of the doped poly-Si contacts. In this context, it is essential to note that research into the localization of doped poly-Si contacts is still in its nascent stage. Several strategies for poly-Si localization have been proposed, such as photolithography,[198] reactive ion etching,[199] laser processing,[200] shadow mask deposition,[201,202] and chemical etch back.[203,204] Shadow mask deposition can be used in combination with a directional deposition method, such as sputtering. Alternatively, the common patterning processes of chemical etch back, and laser processing maybe used when a masking layer is applied on the poly-Si layers, capable of withstanding subsequent chemical etching or laser ablation.

V. CONCLUSION

The advancement of passivating contact solar cell technologies, particularly with doped poly-Si contacts, marks a significant step in the evolution of the PV industry. While n^+ poly-Si contacts have achieved a rapid pace of progress, the comparative lack of progress in p^+ poly-Si contacts performance requires focused research and development efforts. The fundamental limitations of p^+ poly contacts, including segregation of boron in the interfacial oxide and the resulting boron-induced damage have hindered its efficacy compared to n^+ poly-Si contacts. To address these challenges, alternative dopants like Ga have been explored to reduce interface damage, while alternative interfacial layers such as SiO_xN_y have shown promise in improving passivation quality. The adoption of multilayer configurations and pre-annealing techniques also offers potential solutions to optimize p^+ poly-Si contact performance. Meanwhile, the metallization of p^+ poly-Si contacts, particularly using screen-printed and fire-through methods, requires tailored pastes that can create shallow, dense, and small metal crystallites. Therefore, to unlock the full potential of doped poly-Si contacts based passivating contact solar cells, addressing p^+ poly-Si contacts challenges is essential. Collaborative efforts between academia and industry offer promise in overcoming these limitations and advancing efficient and commercially viable fully passivating contact solar cells, thereby improving solar cell technology.

ACKNOWLEDGMENTS

This work has been supported by the Australian Renewable Energy Agency (ARENA) through the Australian Centre for Advanced Photovoltaics (ACAP) and Project Nos. 2022/TRAC004 and 2022/TRAC005.

AUTHOR DECLARATIONS

Conflict of Interest

The authors have no conflicts to disclose.

Author Contributions

Rabin Basnet: Conceptualization (equal); Data curation (equal); Formal analysis (equal); Investigation (equal); Methodology (equal); Writing – original draft (equal); Writing – review & editing (equal). **Di Yan:** Data curation (equal); Methodology (equal); Writing – review & editing (equal). **Di Kang:** Data curation (equal); Investigation (equal); Writing – review & editing (equal). **Mohamed M. Shehata:** Investigation (equal); Visualization (equal); Writing – review & editing

(equal). **Sieu Pheng Phang:** Investigation (equal); Writing – review & editing (equal). **Thien Truong:** Investigation (equal); Writing – review & editing (equal). **James Bullock:** Methodology (equal); Writing – review & editing (equal). **Heping Shen:** Project administration (equal); Writing – review & editing (equal). **Daniel Macdonald:** Conceptualization (equal); Funding acquisition (equal); Methodology (equal); Resources (equal); Supervision (equal); Writing – review & editing (equal).

DATA AVAILABILITY

The data that support the findings of this study are available from the corresponding authors upon reasonable request.

REFERENCES

[1]VDMA (2023). "International technology roadmap for photovoltaic (ITRPV)," https://itrpv.vdma.org/.

[2]M. Hermle, F. Feldmann, M. Bivour, J. C. Goldschmidt, and S. W. Glunz, "Passivating contacts and tandem concepts: Approaches for the highest silicon-based solar cell efficiencies," Appl. Phys. Rev. **7**(2), 21305 (2020).

[3]R. Chen *et al.*, "23.83% efficient mono-PERC incorporating advanced hydrogenation," Prog. Photovoltaics Res. Appl. **28**(12), 1239–1247 (2020).

[4]T. Dullweber and J. Schmidt, "Industrial silicon solar cells applying the passivated emitter and rear cell (PERC) concept—A review," IEEE J. Photovoltaics **6**(5), 1366–1381 (2016).

[5]G. M. Wilson *et al.*, "The 2020 photovoltaic technologies roadmap," J. Phys. D. Appl. Phys. **53**(49), 493001 (2020).

[6]A. Richter *et al.*, "Design rules for high-efficiency both-sides-contacted silicon solar cells with balanced charge carrier transport and recombination losses," Nat. Energy **6**(4), 429–438 (2021).

[7]F. Feldmann, M. Bivour, C. Reichel, M. Hermle, and S. W. Glunz, "Passivated rear contacts for high-efficiency n-type Si solar cells providing high interface passivation quality and excellent transport characteristics," Sol. Energy Mater. Sol. Cells **120**, 270–274 (2014).

[8]K. Yoshikawa *et al.*, "Exceeding conversion efficiency of 26% by heterojunction interdigitated back contact solar cell with thin film Si technology," Sol. Energy Mater. Sol. Cells **173**, 37–42 (2017).

[9]M. Taguchi *et al.*, "24.7% record efficiency HIT solar cell on thin silicon wafer," IEEE J. Photovoltaics **4**(1), 96–99 (2014).

[10]H. Lin *et al.*, "Silicon heterojunction solar cells with up to 26.81% efficiency achieved by electrically optimized nanocrystalline-silicon hole contact layers," Nat. Energy **8**(8), 789–799 (2023).

[11]P. Verlinden *et al.*, "Photovoltaic device innovation for a solar future," Device **1**, 100013 (2023).

[12]U. Römer *et al.*, "Recombination behavior and contact resistance of n+ and p+ poly-crystalline Si/mono-crystalline Si junctions," Sol. Energy Mater. Sol. Cells **131**, 85–91 (2014).

[13]Y. Li *et al.*, "Research of annealing and boron doping on SiO x/p + -poly-Si hole-selective passivated contact," IEEE J. Photovoltaics **10**(6), 1552–1556 (2020).

[14]D. L. Young *et al.*, "Gallium-doped poly-Si:Ga/SiO_2 passivated emitters to n-Cz wafers with iV oc >730 mV," IEEE J. Photovoltaics **7**(6), 1640–1645 (2017).

[15]D. Yan, A. Cuevas, S. P. Phang, Y. Wan, and D. Macdonald, "23% efficient p-type crystalline silicon solar cells with hole-selective passivating contacts based on physical vapor deposition of doped silicon films," Appl. Phys. Lett. **113**(6), 61603 (2018).

[16]Y. Zhi *et al.*, "Ga-doped Czochralski silicon with rear p-type polysilicon passivating contact for high-efficiency p-type solar cells," Sol. Energy Mater. Sol. Cells **230**, 111229 (2021).

[17]X. Guo *et al.*, "Comparison of different types of interfacial oxides on hole-selective p+-poly-Si passivated contacts for high-efficiency c-Si solar cells," Sol. Energy Mater. Sol. Cells **210**, 110487 (2020).

[18]A. Ingenito *et al.*, "Implementation and understanding of p+ fired rear hole selective tunnel oxide passivating contacts enabling >22% conversion efficiency in p-type c-Si solar cells," Sol. Energy Mater. Sol. Cells **219**, 110809 (2021).

[19]S. Mack, M. Lenes, J. Luchies, and A. Wolf, "P-type silicon solar cells with passivating rear contact formed by LPCVD p + polysilicon and screen printed Ag metallization," Phys. Status Solidi – Rapid Res. Lett. **13**(7), 1900064 (2019).

[20]W.-J. Choi *et al.*, "Optimization of in-situ and ex-situ doped p+ passivating contact for high efficiency p-TOPCon solar cell application," in *2021 IEEE 48th Photovoltaic Specialists Conference (PVSC)* (IEEE, 2021), pp. 1907–1912.

[21]H. Xing *et al.*, "Plasma treatment for chemical SiOx enables excellent passivation of p-type polysilicon passivating contact featuring the lowest J of ∼6 fA/cm^2," Sol. Energy Mater. Sol. Cells **257**, 112354 (2023).

[22]D. Ma *et al.*, "Highly improved passivation of PECVD p-type TOPCon by suppressing plasma-oxidation ion-bombardment-induced damages," Sol. Energy **242**, 1–9 (2022).

[23]S. Mack, D. Herrmann, M. Lenes, M. Renes, and A. Wolf, "Progress in p-type tunnel oxide-passivated contact solar cells with screen-printed contacts," Sol. RRL **5**(5), 2100152 (2021).

[24]T. F. Wietler *et al.*, "Pinhole density and contact resistivity of carrier selective junctions with polycrystalline silicon on oxide," Appl. Phys. Lett. **110**(25), 253902 (2017).

[25]R. Peibst *et al.*, "A simple model describing the symmetric I–V characteristics of p polycrystalline Si/n monocrystalline Si, and n polycrystalline Si/p monocrystalline Si junctions," IEEE J. Photovoltaics **4**(3), 841–850 (2014).

[26]D. Yan, A. Cuevas, J. Bullock, Y. Wan, and C. Samundsett, "Phosphorus-diffused polysilicon contacts for solar cells," Sol. Energy Mater. Sol. Cells **142**, 75–82 (2015).

[27]M. K. Stodolny *et al.*, "n-Type polysilicon passivating contact for industrial bifacial n-type solar cells," Sol. Energy Mater. Sol. Cells **158**, 24–28 (2016).

[28]T. Gao *et al.*, "An industrially viable TOPCon structure with both ultra-thin SiOx and n+-poly-Si processed by PECVD for p-type c-Si solar cells," Sol. Energy Mater. Sol. Cells **200**, 109926 (2019).

[29]F. Feldmann *et al.*, "Industrial TOPCon solar cells realized by a PECVD tube process," in *37th European Photovoltaic Solar Energy Conference and Exhibition* (Curran Associates, 2020), pp. 164–169.

[30]A. Moldovan, F. Feldmann, M. Zimmer, J. Rentsch, J. Benick, and M. Hermle, "Tunnel oxide passivated carrier-selective contacts based on ultra-thin SiO_2 layers," Sol. Energy Mater. Sol. Cells **142**, 123–127 (2015).

[31]Y. Huang *et al.*, "Ultrathin silicon oxide prepared by in-line plasma-assisted N_2O oxidation (PANO) and the application for n-type polysilicon passivated contact," Sol. Energy Mater. Sol. Cells **208**, 110389 (2020).

[32]A. Richter *et al.*, "Tunnel oxide passivating electron contacts as full-area rear emitter of high-efficiency p-type silicon solar cells," Prog. Photovoltaics Res. Appl. **26**(8), 579–586 (2018).

[33]B. Steinhauser, J.-I. Polzin, F. Feldmann, M. Hermle, and S. W. Glunz, "Excellent surface passivation quality on crystalline silicon using industrial-scale direct-plasma TOPCon deposition technology," Sol. RRL **2**(7), 1800068 (2018).

[34]B. Liao *et al.*, "Atomic scale controlled tunnel oxide enabled by a novel industrial tube-based PEALD technology with demonstrated commercial TOPCon cell efficiencies > 24," Prog. Photovoltaics Res. Appl. **31**(3), 220–229 (2023).

[35]Y. Tao *et al.*, "Large area tunnel oxide passivated rear contact n -type Si solar cells with 21.2% efficiency," Prog. Photovoltaics Res. Appl. **24**(6), 830–835 (2016).

[36]Y. Larionova *et al.*, "On the recombination behavior of p + -type polysilicon on oxide junctions deposited by different methods on textured and planar surfaces," Phys. Status Solidi **214**(8), 1700058 (2017).

[37]P. Padhamnath, N. Nandakumar, B. J. Kitz, N. Balaji, S. D. M.-J. Naval, and V. Shanmugam, "High-quality doped polycrystalline silicon using low-pressure chemical vapor deposition (LPCVD)," in 12th International Photovoltaic Power Generation and Smart Energy Conference & Exhibition Shanghai, China, 27–29 May 2018, pp. 9–14.

[38]See https://www.trinasolar.com/en-glb/resources/newsroom/trina-solar-breaks-world-record-yet-again-setting-i-topcon-cell-efficiency-255 for Trina Press Release "Trina Solar Breaks World Record Yet Again by Setting i-TOPCon Cell Efficiency at 25.5%" (2022, last accessed July 09, 2023).

[39]See https://www.das-solar.com/en/site/news_details/1046 for DASolar Press Release "Das Solar Announced N-type TOPCon3.0 Technology With High Efficiency of 25.2% in Mass Production" (last accessed July 09, 2023).
[40]See https://www.longi.com/en/news/7477/ for Longi Press Release "LONGi sets record of 25.09% for N-Type TOPCon cell efficiency" (2021, last accessed July 09, 2023).
[41]See https://ir.jinkosolar.com/news-releases/news-release-details/jinkosolars-high-efficiency-n-type-monocrystalline-silicon-2 for JinkoSolar Press Release "JinkoSolar's High-efficiency N-Type Monocrystalline Silicon Solar Cell Sets Our New Record with Maximum Conversion Efficiency of 26.4%" (2022, last accessed July 09, 2023).
[42]A. Richter, J. Benick, F. Feldmann, A. Fell, M. Hermle, and S. W. Glunz, "n-Type Si solar cells with passivating electron contact: Identifying sources for efficiency limitations by wafer thickness and resistivity variation," Sol. Energy Mater. Sol. Cells **173**, 96–105 (2017).
[43]A. Richter *et al.*, "Both sides contacted silicon solar cells: Options for approaching 26% efficiency," in *36th European Photovoltaic Solar Energy Conference and Exhibition* (Curran Associates, 2019), pp. 90–95.
[44]R. Peibst *et al.*, "Implementation of n+ and p+ POLO junctions on front and rear side of double-side contacted industrial silicon solar cells," in *32nd European Photovoltaic Solar Energy Conference and Exhibition, Munich, Germany, 20-24 June 2016* (Curran Associates, 2016), pp. 323–327.
[45]P. Zheng *et al.*, "Polysilicon passivating contacts in mass production: The pursuit of higher efficiencies," IEEE J. Photovoltaics **14**(1), 80–84 (2024).
[46]R. Peibst *et al.*, "Towards 28%-efficient Si single-junction solar cells with better passivating POLO junctions and photonic crystals," Sol. Energy Mater. Sol. Cells **238**, 111560 (2022).
[47]F. Feldmann, M. Simon, M. Bivour, C. Reichel, M. Hermle, and S. W. Glunz, "Efficient carrier-selective p- and n-contacts for Si solar cells," Sol. Energy Mater. Sol. Cells **131**, 100–104 (2014).
[48]E. Bellini (2023). "Jolywood claims 26.7% efficiency for n-type TOPCon solar cell," pv magazine. https://www.pv-magazine.com/2023/04/12/jolywood-claims-26-7-efficiency-for-n-type-topcon-solar-cell/
[49]N. Lin *et al.*, "Excellent surface passivation of p-type TOPCon enabled by ozone-gas oxidation with a single-sided saturation current density of ~ 4.5 fA/cm^2," Sol. Energy **259**, 348–355 (2023).
[50]C. Madumelu *et al.*, "Assessing the stability of p+ and n+ polysilicon passivating contacts with various capping layers on p-type wafers," Sol. Energy Mater. Sol. Cells **253**, 112245 (2023).
[51]C. Guo *et al.*, "Influence of backside surface morphology on passivation and contact characteristics of TOPCON solar cells," Sol. Energy **258**, 278–288 (2023).
[52]S. Kim *et al.*, "Bi-polysilicon passivating contact technique for crystalline silicon solar cell," Mater. Sci. Semicond. Process **160**, 107453 (2023).
[53]P. J. Dale and M. A. Scarpulla, "Efficiency versus effort: A better way to compare best photovoltaic research cell efficiencies?," Sol. Energy Mater. Sol. Cells **251**, 112097 (2023).
[54]M. Lu *et al.*, "Screen-printable conductor metallizations for industrial n-TOPCon crystalline silicon solar cells," in *2021 IEEE 48th Photovoltaic Specialists Conference (PVSC)* (IEEE, 2021), pp. 0954–0957.
[55]K. Madani, A. Rohatgi, B. Rounsaville, M.-G. Kang, H.-E. Song, and Y.-W. Ok, "Enhanced stability of exposed PECVD grown thin n + poly-Si/SiO x passivating contacts with Al_2O_3 capping layer during high temperature firing," IEEE J. Photovoltaics **11**(2), 268–272 (2021).
[56]Y.-Y. Huang, Y.-W. Ok, A. D. Upadhyaya, V. D. Upadhyaya, K. Madani, and A. Rohatgi, "Large area 21.6% efficiency front junction N-type cell with screen printed tunnel oxide passivated poly-Si rear contact," in *2019 IEEE 46th Photovoltaic Specialists Conference (PVSC)* (IEEE, 2019), pp. 1120–1123.
[57]B. Steinhauser *et al.*, "Large area TOPCon technology achieving 23.4% efficiency," in *2018 IEEE 7th World Conference on Photovoltaic Energy Conversion (WCPEC) (a Joint Conference of 45th IEEE PVSC, 28th PVSEC & 34th EU PVSEC)* (IEEE, 2018), pp. 1507–1510.
[58]Y. Tao, K. Madani, E. Cho, B. Rounsaville, V. Upadhyaya, and A. Rohatgi, "High-efficiency selective boron emitter formed by wet chemical etch-back for n -type screen-printed Si solar cells," Appl. Phys. Lett. **110**(2), 021101 (2017).
[59]Y. Zhou *et al.*, "Screen-printed n-type industry solar cells with tunnel oxide passivated contact doped by phosphorus diffusion," Superlattices Microstruct. **148**, 106720 (2020).
[60]Q. Wang *et al.*, "Study on the cleaning process of n+-poly-Si wraparound removal of TOPCon solar cells," Sol. Energy **211**, 324–335 (2020).
[61]Y.-Y. Huang *et al.*, "Fully screen-printed bifacial large area 22.6% N-type Si solar cell with lightly doped ion-implanted boron emitter and tunnel oxide passivated rear contact," Sol. Energy Mater. Sol. Cells **214**, 110585 (2020).
[62]Y. Zhou *et al.*, "The impacts of LPCVD wrap-around on the performance of n-type tunnel oxide passivated contact c-Si solar cell," Curr. Appl. Phys. **20**(7), 911–916 (2020).
[63]Q. Yang *et al.*, "In-situ phosphorus-doped polysilicon prepared using rapid-thermal anneal (RTA) and its application for polysilicon passivated-contact solar cells," Sol. Energy Mater. Sol. Cells **210**, 110518 (2020).
[64]D. Chen *et al.*, "24.58% total area efficiency of screen-printed, large area industrial silicon solar cells with the tunnel oxide passivated contacts (i-TOPCon) design," Sol. Energy Mater. Sol. Cells **206**, 110258 (2020).
[65]W. Chen *et al.*, "Influence of rear surface pyramid base microstructure on industrial n-TOPCon solar cell performances," Sol. Energy **247**, 24–31 (2022).
[66]T. Fellmeth *et al.*, "Laser-enhanced contact optimization on i TOPCon solar cells," Prog. Photovoltaics Res. Appl. **30**(12), 1393–1399 (2022).
[67]Q. Wang *et al.*, "High-efficiency n-TOPCon bifacial solar cells with selective poly-Si based passivating contacts," Sol. Energy Mater. Sol. Cells **259**, 112458 (2023).
[68]H. Du *et al.*, "24.18% efficiency TOPCon solar cells enabled by super hydrophilic carbon-doped polysilicon films combined with plated metal fingers," Sol. Energy Mater. Sol. Cells **257**, 112393 (2023).
[69]W. Chen *et al.*, "Enhancing industrialization TOPCon solar cell efficiency via comprehensive anti-reflection passivation film optimization," Mater. Sci. Semicond. Process **169**, 107874 (2024).
[70]S. Ma *et al.*, "24.7% industrial tunnel oxide passivated contact solar cells prepared through tube PECVD integrating with plasma-assisted oxygen oxidation and in-situ doped polysilicon," Sol. Energy Mater. Sol. Cells **257**, 112396 (2023).
[71]G. Nogay *et al.*, "Interplay of annealing temperature and doping in hole selective rear contacts based on silicon-rich silicon-carbide thin films," Sol. Energy Mater. Sol. Cells **173**, 18–24 (2017).
[72]M. Q. Khokhar *et al.*, "A review on p-type tunnel oxide passivated contact (TOPCon) solar cell," Trans. Electr. Electron. Mater. **24**(3), 2100152 (2023).
[73]J. Zhou *et al.*, "Recent advancements in poly-Si/SiO x passivating contacts for high-efficiency silicon solar cells: Technology review and perspectives," J. Mater. Chem. A **10**(38), 20147–20173 (2022).
[74]S. W. Glunz *et al.*, "Silicon-based passivating contacts: The TOPCon route," Prog. Photovoltaics Res. Appl. **31**(4), 341–359 (2023).
[75]D. Yan *et al.*, "Polysilicon passivated junctions: The next technology for silicon solar cells?," Joule **5**(4), 811–828 (2021).
[76]T. G. Allen, J. Bullock, X. Yang, A. Javey, and S. De Wolf, "Passivating contacts for crystalline silicon solar cells," Nat. Energy **4**(11), 914–928 (2019).
[77]F. Feldmann, C. Reichel, R. Müller, and M. Hermle, "The application of poly-Si/SiOx contacts as passivated top/rear contacts in Si solar cells," Sol. Energy Mater. Sol. Cells **159**, 265–271 (2017).
[78]A. Morisset *et al.*, "Highly passivating and blister-free hole selective polysilicon based contact for large area crystalline silicon solar cells," Sol. Energy Mater. Sol. Cells **200**, 109912 (2019).
[79]M. Hayes, B. Martel, S. Dubois, A. Morisset, and O. Palais, "Study of non fire-through metallization processes of boron-doped polysilicon passivated contacts for high efficiency silicon solar cells," AIP Conf. Proc. **2147**(1), 40006 (2019).
[80]A. Morisset *et al.*, "Conductivity and surface passivation properties of boron-doped poly-silicon passivated contacts for c-Si solar cells," Phys. Status Solidi **216**(10), 1800603 (2019).
[81]M. Hayes *et al.*, "Impurity gettering by boron- and phosphorus-doped polysilicon passivating contacts for high-efficiency multicrystalline silicon solar cells," Phys. Status Solidi **216**(17), 1900321 (2019).
[82]F. Feldmann, J. Schön, J. Niess, W. Lerch, and M. Hermle, "Studying dopant diffusion from Poly-Si passivating contacts," Sol. Energy Mater. Sol. Cells **200**, 109978 (2019).

[83]K. Inoue *et al.*, "Dopant distribution in gate electrode of n- and p-type metal-oxide-semiconductor field effect transistor by laser-assisted atom probe," Appl. Phys. Lett. **95**(4), 43502 (2009).
[84]F. Feldmann, R. Müller, C. Reichel, and M. Hermle, "Ion implantation into amorphous Si layers to form carrier-selective contacts for Si solar cells," Phys. Status Solidi - Rapid Res. Lett. **8**(9), 767–770 (2014).
[85]B. W. H. van de Loo *et al.*, "On the hydrogenation of Poly-Si passivating contacts by Al_2O_3 and SiN thin films," Sol. Energy Mater. Sol. Cells **215**, 110592 (2020).
[86]D. L. Young *et al.*, "Interdigitated back passivated contact (IBPC) solar cells formed by ion implantation," IEEE J. Photovoltaics **6**(1), 41–47 (2016).
[87]N. Nandakumar *et al.*, "Approaching 23% with large-area monoPoly cells using screen-printed and fired rear passivating contacts fabricated by inline PECVD," Prog. Photovoltaics Res. Appl. **27**(2), 107–112 (2018).
[88]K. C. Fong *et al.*, "Phosphorus diffused LPCVD polysilicon passivated contacts with in-situ low pressure oxidation," Sol. Energy Mater. Sol. Cells **186**, 236–242 (2018).
[89]P. Padhamnath *et al.*, "Development of thin polysilicon layers for application in monoPoly^{TM} cells with screen-printed and fired metallization," Sol. Energy Mater. Sol. Cells **207**, 110358 (2020).
[90]F. Haase *et al.*, "Laser contact openings for local poly-Si-metal contacts enabling 26.1%-efficient POLO-IBC solar cells," Sol. Energy Mater. Sol. Cells **186**, 184–193 (2018).
[91]W. Chen, W. Liu, Y. Yu, P. Chen, and Y. Wan, "A study of activated phosphorus distribution within silicon substrate for polysilicon passivating contacts based on an in-line PVD system," Sol. Energy **259**, 375–380 (2023).
[92]W. Chen, X. Liu, W. Liu, Y. Yu, W. Wang, and Y. Wan, "Optimization of activated phosphorus concentration in recrystallized polysilicon layers for the n-TOPCon solar cell application," Sol. Energy Mater. Sol. Cells **252**, 112206 (2023).
[93]Z. Liu *et al.*, "24.4% industrial tunnel oxide passivated contact solar cells with ozone-gas oxidation nano SiOx and tube PECVD prepared in-situ doped polysilicon," Sol. Energy Mater. Sol. Cells **243**, 111803 (2022).
[94]J. Linke, J. Hoß, F. Buchholz, J. Lossen, and R. Kopecek, "Influence of the annealing temperature of (n) poly-Si/SiOx passivating contacts on their firing stability," Sol. Energy Mater. Sol. Cells **258**, 112415 (2023).
[95]S. Mack, J. Schube, T. Fellmeth, F. Feldmann, M. Lenes, and J.-M. Luchies, "Metallisation of boron-doped polysilicon layers by screen printed silver pastes," Phys. Status Solidi - Rapid Res. Lett. **11**(12), 1700334 (2017).
[96]M. K. Stodolny *et al.*, "Novel schemes of P+ poly-Si hydrogenation implemented in industrial 6" bifacial front-and-rear passivating contacts soalr cells," in *35th European Photovoltaic Solar Energy Conference and Exhibition* (Curran Associates, 2018), pp. 414–417.
[97]Y. Tao, V. Upadhyaya, Y.-Y. Huang, C.-W. Chen, K. Jones, and A. Rohatgi, "Carrier selective tunnel oxide passivated contact enabling 21.4% efficient large-area N-type silicon solar cells," in *2016 IEEE 43rd Photovoltaic Specialists Conference (PVSC)* (IEEE, 2016), pp. 2531–2535.
[98]B. Nemeth *et al.*, "Polycrystalline silicon passivated tunneling contacts for high efficiency silicon solar cells," J. Mater. Res. **31**(6), 671–681 (2016).
[99]A. Merkle *et al.*, "Atmospheric pressure chemical vapor deposition of in-situ doped amorphous silicon layers for passivating contacts," in *35th European Photovoltaic Solar Energy Conference and Exhibition*, Brussels, Belgium, 24–28 September 2018 (Curran Associates, 2018), pp. 785–791.
[100]E. Khorani, T. E. Scheul, A. Tarazona, J. Nutter, T. Rahman, and S. A. Boden, "p+ polycrystalline silicon growth via hot wire chemical vapour deposition for silicon solar cells," Thin Solid Films **705**, 137978 (2020).
[101]T. N. Truong *et al.*, "Deposition pressure dependent structural and opto-electronic properties of ex-situ boron-doped poly-Si/SiOx passivating contacts based on sputtered silicon," Sol. Energy Mater. Sol. Cells **215**, 110602 (2020).
[102]Z. Xin *et al.*, "Ultra-thin atomic layer deposited aluminium oxide tunnel layer passivated hole-selective contacts for silicon solar cells," Sol. Energy Mater. Sol. Cells **191**, 164–174 (2019).
[103]Z. Yang *et al.*, "Comparing the gettering effect of heavily doped polysilicon films and its implications for tunnel oxide-passivated contact solar cells," Sol. RRL **7**(8), 2200578 (2023).
[104]J. Stuckelberger *et al.*, "Pre-annealing for improved LPCVD deposited boron-doped poly-Si hole-selective contacts," Sol. Energy Mater. Sol. Cells **251**, 112123 (2023).
[105]H. Park *et al.*, "Boron-doped polysilicon using spin-on doping for high-efficiency both-side passivating contact silicon solar cells," Prog. Photovoltaics Res. Appl. **31**(5), 461–473 (2023).
[106]Z. Ding *et al.*, "Boron spin-on doping for poly-Si/SiOx passivating contacts," ACS Appl. Energy Mater. **4**(5), 4993–4999 (2021).
[107]T. N. Truong *et al.*, "Investigation of gallium–boron spin-on codoping for poly-Si/SiOx passivating contacts," Sol. RRL **5**(12), 2100653 (2021).
[108]A. H. Soeriyadi *et al.*, "Impact of firing and capping layers on long-term stability of doped poly-Si passivating contact layers," AIP Conf. Proc. **2487**(1), 50006 (2022).
[109]J.-I. Polzin, F. Feldmann, B. Steinhauser, M. Bivour, and M. Hermle, "Annealing and firing stability of in situ Boron-doped poly-Si passivating contacts," AIP Conf. Proc. **2826**(1), 20007 (2023).
[110]M. Schnabel *et al.*, "Hydrogen passivation of poly-Si/SiOx contacts for Si solar cells using Al_2O_3 studied with deuterium," Appl. Phys. Lett. **112**(20), 203901 (2018).
[111]T. N. Truong *et al.*, "Hydrogenation of phosphorus-doped polycrystalline silicon films for passivating contact solar cells," ACS Appl. Mater. Interfaces **11**(5), 5554–5560 (2019).
[112]D. Kang *et al.*, "Optimum hydrogen injection in phosphorus-doped polysilicon passivating contacts," ACS Appl. Mater. Interfaces **13**(46), 55164–55171 (2021).
[113]C. Hollemann *et al.*, "Changes in hydrogen concentration and defect state density at the poly-Si/SiOx/c-Si interface due to firing," Sol. Energy Mater. Sol. Cells **231**, 111297 (2021).
[114]D. Kang *et al.*, "Comparison of firing stability between p- and n-type polysilicon passivating contacts," Prog. Photovoltaics Res. Appl. **30**(8), 970–980 (2022).
[115]B. J. Hallam *et al.*, "Overcoming the challenges of hydrogenation in silicon solar cells," Aust. J. Chem. **71**(10), 743 (2018).
[116]D. Mathiot, "Modeling of hydrogen diffusion in n - and p -type silicon," Phys. Rev. B **40**(8), 5867–5870 (1989).
[117]A. Van Wieringen and N. Warmoltz, "On the permeation of hydrogen and helium in single crystal silicon and germanium at elevated temperatures," Physica **22**(6–12), 849–865 (1956).
[118]P. Hamer *et al.*, "Hydrogen induced contact resistance in PERC solar cells," Sol. Energy Mater. Sol. Cells **184**, 91–97 (2018).
[119]K. Chen *et al.*, "Pulsed laser annealed Ga hyperdoped poly-Si SiO_x passivating contacts for high-efficiency monocrystalline Si solar cells," Energy Environ. Mater. **6**(3), e12542 (2023).
[120]Y.-W. Ok *et al.*, "Screen printed, large area bifacial N-type back junction silicon solar cells with selective phosphorus front surface field and boron doped poly-Si/SiOx passivated rear emitter," Appl. Phys. Lett. **113**(26), 263901 (2018).
[121]P. Padhamnath, N. Nampalli, A. Khanna, B. Nagarajan, A. G. Aberle, and S. Duttagupta, "Progress with passivation and screen-printed metallization of Boron-doped monoPoly^{TM} layers," Sol. Energy **231**, 8–26 (2022).
[122]P. Padhamnath *et al.*, "Characterization of screen printed and fire-through contacts on LPCVD based passivating contacts in monoPoly^{TM} solar cells," Sol. Energy **202**, 73–79 (2020).
[123]R. Peibst *et al.*, "Building blocks for industrial, screen-printed double-side contacted POLO cells with highly transparent ZnO:Al layers," IEEE J. Photovoltaics **8**(3), 1–7 (2018).
[124]F. Haase *et al.*, "Interdigitated back contact solar cells with polycrystalline silicon on oxide passivating contacts for both polarities," Jpn. J. Appl. Phys. **56**(8S2), 08MB15 (2017).
[125]H. E. Çiftpınar *et al.*, "Study of screen printed metallization for polysilicon based passivating contacts," Energy Proc. **124**, 851–861 (2017).
[126]J. Bao *et al.*, "Towards 24% efficiency for industrialn-type bifacial passivating-contact solar cells with homogeneous emitter," in *Proceedings of the 37th European Photovoltaic Conference (EUPVSEC)* (WIP Renewable Energies, 2020), pp. 160–163.
[127]A. Liu *et al.*, "Understanding the impurity gettering effect of polysilicon/oxide passivating contact structures through experiment and simulation," Sol. Energy Mater. Sol. Cells **230**, 111254 (2021).

[128]A. Liu, D. Yan, S. P. Phang, A. Cuevas, and D. Macdonald, "Effective impurity gettering by phosphorus- and boron-diffused polysilicon passivating contacts for silicon solar cells," Sol. Energy Mater. Sol. Cells **179**, 136–141 (2018).
[129]Z. Yang *et al.*, "Impurity gettering in polycrystalline-silicon based passivating contacts—The role of oxide stoichiometry and pinholes," Adv. Energy Mater **12**(24), 2103773 (2022).
[130]A. S. Grove, O. Leistiko, and C. T. Sah, "Redistribution of acceptor and donor impurities during thermal oxidation of silicon," J. Appl. Phys. **35**(9), 2695–2701 (1964).
[131]T. Yamamoto, K. Uwasawa, and T. Mogami, "Bias temperature instability in scaled p/sup +/polysilicon gate p-MOSFET's," IEEE Trans. Electron Devices **46**(5), 921–926 (1999).
[132]Y. J. Oh, H.-K. Noh, and K. J. Chang, "First-principles study of the segregation of boron dopants near the interface between crystalline Si and amorphous SiO_2," Phys. B Condens. Matter **407**(15), 2989–2992 (2012).
[133]C.-M. Lin, A. J. Steckl, and T. P. Chow, "Electrical properties of Ga-implanted Si p/sup +/-n shallow junctions fabricated by low-temperature rapid thermal annealing," IEEE Electron Device Lett. **9**(11), 594–597 (1988).
[134]S. W. Jones, *Diffusion in Silicon* (IC Knowledge LLC, 2008).
[135]A. S. Grove, O. Leistiko, and C. T. Sah, "Diffusion of gallium through a silicon dioxide layer," J. Phys. Chem. Solids **25**(9), 985–992 (1964).
[136]G. L. Vick and K. M. Whittle, "Solid solubility and diffusion coefficients of boron in silicon," J. Electrochem. Soc. **116**(8), 1142 (1969).
[137]V. E. Boeisenko and S. G. Yudin, "Steady-state solubility of substitutional impurities in silicon," Phys. Status Solidi **101**(1), 123–127 (1987).
[138]C. W. White, S. R. Wilson, B. R. Appleton, and F. W. Young, "Supersaturated substitutional alloys formed by ion implantation and pulsed laser annealing of group-III and group-V dopants in silicon," J. Appl. Phys. **51**(1), 738–749 (1980).
[139]A. Casel, H. Jorke, E. Kasper, and H. Kibbel, "Dependence of hole transport on Ga doping in Si molecular beam epitaxy layers," Appl. Phys. Lett. **48**(14), 922–924 (1986).
[140]H. B. Harrison, S. S. Iyer, G. A. Sai-Halasz, and S. A. Cohen, "Highly activated shallow Ga profiles in silicon obtained by implantation and rapid thermal annealing," Appl. Phys. Lett. **51**(13), 992–994 (1987).
[141]H. Steinkemper, F. Feldmann, M. Bivour, and M. Hermle, "Numerical simulation of carrier-selective electron contacts featuring tunnel oxides," IEEE J. Photovoltaics **5**(5), 1348–1356 (2015).
[142]R. Peibst *et al.*, "Working principle of carrier selective poly-Si/c-Si junctions: Is tunnelling the whole story?," Sol. Energy Mater. Sol. Cells **158**, 60–67 (2016).
[143]W. Liu *et al.*, "Polysilicon passivating contacts for silicon solar cells: Interface passivation and carrier transport mechanism," ACS Appl. Energy Mater. **2**(7), 4609–4617 (2019).
[144]A. S. Kale *et al.*, "Understanding the charge transport mechanisms through ultrathin SiO x layers in passivated contacts for high-efficiency silicon solar cells," Appl. Phys. Lett. **114**(8), 083902 (2019).
[145]S. Choi *et al.*, "Structural evolution of tunneling oxide passivating contact upon thermal annealing," Sci. Rep. **7**(1), 12853 (2017).
[146]C. Hollemann *et al.*, "Separating the two polarities of the POLO contacts of an 26.1%-efficient IBC solar cell," Sci. Rep. **10**(1), 658 (2020).
[147]J. Krügener, F. Haase, M. Rienäcker, R. Brendel, H. J. Osten, and R. Peibst, "Improvement of the SRH bulk lifetime upon formation of n-type POLO junctions for 25% efficient Si solar cells," Sol. Energy Mater. Sol. Cells **173**, 85–91 (2017).
[148]H. Du *et al.*, "Concurrently preparing front emitter and rear passivating contact via continuous PECVD deposition plus one-step annealing for high-efficiency tunnel oxide passivating contact solar cells," Sol. RRL **7**(7), 2201082 (2023).
[149]C. Reichel, F. Feldmann, A. Richter, J. Benick, M. Hermle, and S. W. Glunz, "Polysilicon contact structures for silicon solar cells using atomic layer deposited oxides and nitrides as ultra-thin dielectric interlayers," Prog. Photovoltaics Res. Appl. **30**(3), 288–299 (2022).
[150]G. Kaur, Z. Xin, R. Sridharan, A. Danner, and R. Stangl, "Engineering aluminum oxide/polysilicon hole selective passivated contacts for high efficiency solar cells," Sol. Energy Mater. Sol. Cells **218**, 110758 (2020).
[151]R. S. Bonilla, I. Al-Dhahir, M. Yu, P. Hamer, and P. P. Altermatt, "Charge fluctuations at the Si–SiO_2 interface and its effect on surface recombination in solar cells," Sol. Energy Mater. Sol. Cells **215**, 110649 (2020).
[152]J. L. Alay and M. Hirose, "The valence band alignment at ultrathin SiO_2/Si interfaces," J. Appl. Phys. **81**(3), 1606–1608 (1997).
[153]M. Depas, B. Vermeire, P. Mertens, R. Van Meirhaeghe, and M. Heyns, "Determination of tunnelling parameters in ultra-thin oxide layer poly-Si/SiO_2/Si structures," Solid. State. Electron **38**(8), 1465–1471 (1995).
[154]R. Kumar Chanana, "Determination of hole effective mass in SiO_2 and SiC conduction band offset using Fowler–Nordheim tunneling characteristics across metal-oxide-semiconductor structures after applying oxide field corrections," J. Appl. Phys. **109**(10), 104508 (2011).
[155]J. W. Keister, J. E. Rowe, J. J. Kolodziej, H. Niimi, T. E. Madey, and G. Lucovsky, "Band offsets for ultrathin SiO [sub 2] and Si [sub 3]N [sub 4] films on Si(111) and Si(100) from photoemission spectroscopy," J. Vac. Sci. Technol. B, Microelectron. Nanom. Struct. **17**(4), 1831 (1999).
[156]E. Bersch, S. Rangan, R. A. Bartynski, E. Garfunkel, and E. Vescovo, "Band offsets of ultrathin high-k oxide films with Si," Phys. Rev. B **78**(8), 85114 (2008).
[157]S. McNab *et al.*, "Alternative dielectrics for hole selective passivating contacts and the influence of nanolayer built-in charge," AIP Conf. Proc. **2487**(1), 20013 (2022).
[158]E. Khorani *et al.*, "Optoelectronic properties of ultrathin ALD silicon nitride and its potential as a hole-selective nanolayer for high efficiency solar cells," APL Mater. **8**(11), 111106 (2020).
[159]M. Lozac'h, S. Nunomura, and K. Matsubara, "Double-sided TOPCon solar cells on textured wafer with ALD SiOx layer," Sol. Energy Mater. Sol. Cells **207**, 110357 (2020).
[160]H. Hwang, W. Ting, D.-L. Kwong, and J. Lee, "A physical model for boron penetration through an oxynitride gate dielectric prepared by rapid thermal processing in N_2O," Appl. Phys. Lett. **59**(13), 1581–1582 (1991).
[161]D. Mathiot, A. Straboni, E. Andre, and P. Debenest, "Boron diffusion through thin gate oxides: Influence of nitridation and effect on the Si/SiO_2 interface electrical characteristics," J. Appl. Phys. **73**(12), 8215–8220 (1993).
[162]T. Morimoto, H. S. Momose, Y. Ozawa, K. Yamabe, and H. Iwai, "Effects of boron penetration and resultant limitations in ultra thin pure-oxide and nitrided-oxide gate-films," in *International Technical Digest on Electron Devices* (IEEE, 1990), pp. 429–432.
[163]D. P. Pham *et al.*, "Innovative passivating contact using quantum well at poly-Si/c-Si interface for crystalline silicon solar cells," Chem. Eng. J. **423**, 130239 (2021).
[164]P. Wyss *et al.*, "A mixed-phase SiOx hole selective junction compatible with high temperatures used in industrial solar cell manufacturing," IEEE J. Photovoltaics **10**(5), 1262–1269 (2020).
[165]J.-I. Polzin, F. Feldmann, B. Steinhauser, M. Hermle, and S. W. Glunz, "Study on the interfacial oxide in passivating contacts," AIP Conf. Proc. **2147**(1), 040016 (2019).
[166]G. Yang *et al.*, "Will SiO -pinholes for SiO/poly-Si passivating contact enhance the passivation quality?," Sol. Energy Mater. Sol. Cells **252**, 112200 (2023).
[167]M. Fırat *et al.*, "Local enhancement of dopant diffusion from polycrystalline silicon passivating contacts," ACS Appl. Mater. Interfaces **14**(15), 17975–17986 (2022).
[168]S. Kalainathan, R. Dhanasekaran, and P. Ramasamy, "Grain growth mechanism in heavily arsenic-doped polycrystalline silicon," J. Mater. Sci. Mater. Electron. **2**(2), 98–104 (1991).
[169]L. Mei, M. Rivier, Y. Kwark, and R. W. Dutton, "Grain-growth mechanisms in polysilicon," J. Electrochem. Soc. **129**(8), 1791–1795 (1982).
[170]A. R. Sitaram, S. P. Murarka, and T. T. Sheng, "Grain growth in boron doped LPCVD polysilicon films," J. Mater. Res. **5**(2), 360–364 (1990).
[171]H.-J. Kim and C. V. Thompson, "The effects of dopants on surface-energy-driven secondary grain growth in silicon films," J. Appl. Phys. **67**(2), 757–767 (1990).
[172]H. Massoud, "Thermal oxidation of silicon in the ultrathin regime," Solid. State. Electron. **41**(7), 929–934 (1997).
[173]A. S. Kale *et al.*, "Modifications of textured silicon surface morphology and its effect on poly-Si/SiOx contact passivation for silicon solar cells," IEEE J. Photovoltaics **9**(6), 1513–1521 (2019).
[174]A. S. Kale *et al.*, "Effect of crystallographic orientation and nanoscale surface morphology on poly-Si/SiOx contacts for silicon solar cells," ACS Appl. Mater. Interfaces **11**(45), 42021–42031 (2019).

[175]Y. Kato, H. Takao, K. Sawada, and M. Ishida, "Improvement of metal-oxide semiconductor interface characteristics in complementary metal-oxide semiconductor on Si(111) by combination of fluorine implantation and long-time hydrogen annealing," Jpn. J. Appl. Phys. **45**(4), L108 (2006).
[176]J. A. Cooper and R. J. Schwartz, "Electrical characteristics of the SiO_2-Si interface near midgap and in weak inversion," Solid State Electron. **17**(7), 641–654 (1974).
[177]J.-H. Woo *et al.*, "Critical bending radius of thin single-crystalline silicon with dome and pyramid surface texturing," Scr. Mater. **140**, 1–4 (2017).
[178]P. Gundel, M. C. Schubert, F. D. Heinz, and W. Warta, "Recombination activity enhancement by stress in silicon," in *2010 35th IEEE Photovoltaic Specialists Conference* (IEEE, 2010), pp. 001696–001700.
[179]V. Moroz, N. Strecker, X. Xu, L. Smith, and I. Bork, "Modeling the impact of stress on silicon processes and devices," Mater. Sci. Semicond. Process. **6**(1–3), 27–36 (2003).
[180]S. Mack, F. Feldmann, A. Moldovan, M. Lenes, J. M. Luchies, and A. Wolf, "Impact of surface morphlogy and intterfacial oxide thickness on passivation quality of p+ polysilicon passivating contacts," in *35th European Photovoltaic Solar Energy Conference and Exhibition*, Brussels, Belgium, 24–28 September 2018 (Curran Associates, 2018).
[181]M. Lozac'h and S. Nunomura, "Role of silicon surface, polished ⟨100⟩ and ⟨111⟩ or textured, on the efficiency of double-sided TOPCon solar cells," Prog. Photovoltaics Res. Appl. **28**(10), 1001–1011 (2020).
[182]M. Lozac'h, S. Nunomura, H. Sai, and K. Matsubara, "Passivation property of ultrathin SiOx:H/a-Si:H stack layers for solar cell applications," Sol. Energy Mater. Sol. Cells **185**, 8–15 (2018).
[183]M. Fırat *et al.*, "Large-area bifacial n-TOPCon solar cells with in situ phosphorus-doped LPCVD poly-Si passivating contacts," Sol. Energy Mater. Sol. Cells **236**, 111544 (2022).
[184]N. Zin *et al.*, "Rounded rear pyramidal texture for high efficiency silicon solar cells," in *2016 IEEE 43rd Photovoltaic Specialists Conference (PVSC)* (IEEE, 2016), pp. 2548–2553.
[185]J. B. Heng *et al.*, "23% high-efficiency tunnel oxide junction bifacial solar cell with electroplated Cu gridlines," IEEE J. Photovoltaics **5**(1), 82–86 (2015).
[186]C. Voz, D. Peiró, J. Bertomeu, D. Soler, M. Fonrodona, and J. Andreu, "Optimisation of doped microcrystalline silicon films deposited at very low temperatures by hot-wire CVD," Mater. Sci. Eng. B **69–70**, 278–283 (2000).
[187]R. Lago *et al.*, "Screen printing metallization of boron emitters," Prog. Photovoltaics Res. Appl. **18**(1), 20–27 (2010).
[188]M. B. Field and L. R. Scudder, "Application of thick-film technology to solar cell fabrication," in *12th IEEE Photovoltaic Specialists Conference* (IEEE, 1976), pp. 303–308.
[189]H. Kerp *et al.*, "Development of screen printable contacts for p + emitters in bifacial solar cells," in *21st European Photovoltaic Solar Energy Conference, Dresden, Germany, 4-8 September 2006* (WIP Renewable Energies, 2006), pp. 892–894.
[190]P. Padhamnath, A. Khanna, N. Nandakumar, A. G. Aberle, and S. Duttagupta, "Impact of firing temperature on fire-through metal contacts to P-doped (n) and B-doped (p) poly-Si," Sol. Energy Mater. Sol. Cells **230**, 111217 (2021).
[191]J. Bao *et al.*, "Towards 24% efficiency for industrial n-type bifacial passivating-contact solar cells with homogeneous emitter," in *37th European Photovoltaic Solar Energy Conference and Exhibition* (Curran Associates, 2020), pp. 160–163.
[192]B. Hallam *et al.*, "The silver learning curve for photovoltaics and projected silver demand for net-zero emissions by 2050," Prog. Photovoltaics Res. Appl. **31**(6), 598–606 (2023).
[193]Y. Zhang, M. Kim, L. Wang, P. Verlinden, and B. Hallam, "Design considerations for multi-terawatt scale manufacturing of existing and future photovoltaic technologies: Challenges and opportunities related to silver, indium and bismuth consumption," Energy Environ. Sci. **14**(11), 5587–5610 (2021).
[194]B. Grubel *et al.*, "Direct contact electroplating sequence without initial seed layer for bifacial TOPCon solar cell metallization," IEEE J. Photovoltaics **11**(3), 584–590 (2021).
[195]H. Shen *et al.*, "In situ recombination junction between p-Si and TiO_2 enables high-efficiency monolithic perovskite/Si tandem cells," Sci. Adv. **4**(12), eaau9711 (2018).
[196]H. Shen *et al.*, "Monolithic perovskite/Si tandem solar cells: Pathways to over 30% efficiency," Adv. Energy Mater. **10**(13), 1902840 (2020).
[197]G. Nogay *et al.*, "25.1%-efficient monolithic perovskite/silicon tandem solar cell based on a p-type monocrystalline textured silicon wafer and high-temperature passivating contacts," ACS Energy Lett. **4**(4), 844–845 (2019).
[198]A. Ingenito *et al.*, "Silicon solar cell architecture with front selective and rear full area ion-implanted passivating contacts," Sol. RRL **1**(7), 1700040 (2017).
[199]D. L. Young *et al.*, "Reactive ion etched, self-aligned, selective area poly-Si/SiO_2 passivated contacts," Sol. Energy Mater. Sol. Cells **217**, 110621 (2020).
[200]S. Schäfer *et al.*, "Role of oxygen in the UV-ps laser triggered amorphization of poly-Si for Si solar cells with local passivated contacts," J. Appl. Phys. **129**(13), 133103 (2021).
[201]F. Meyer *et al.*, "Localisation of front side passivating contacts for direct metallisation of high-efficiency c-Si solar cells," Sol. Energy Mater. Sol. Cells **235**, 111455 (2022).
[202]T. Dullweber *et al.*, "Evolutionary PERC+ solar cell efficiency projection towards 24% evaluating shadow-mask-deposited poly-Si fingers below the Ag front contact as next improvement step," Sol. Energy Mater. Sol. Cells **212**, 110586 (2020).
[203]K. Chen *et al.*, "Self-aligned selective area front contacts on poly-Si/SiOx passivating contact c-Si solar cells," IEEE J. Photovoltaics **12**(3), 678–689 (2022).
[204]H. Park *et al.*, "Role of polysilicon in poly-Si/SiOx passivating contacts for high-efficiency silicon solar cells," RSC Adv. **9**(40), 23261–23266 (2019).